

Partitioned coupling of advection–diffusion–reaction systems and Brinkman flows



Pietro Lenarda^a, Marco Paggi^a, Ricardo Ruiz Baier^{b,*}

^a Research Unit on Multi-Scale Analysis of Materials (MUSAM), IMT School for Advances Studies Lucca, Piazza San Francesco 19, 55100 Lucca, Italy

^b Mathematical Institute, University of Oxford, A. Wiles Building, Radcliffe Observatory Quarter, Woodstock Road, Oxford OX2 6GG, UK

ARTICLE INFO

Article history:

Received 23 November 2016

Received in revised form 18 March 2017

Accepted 7 May 2017

Available online 12 May 2017

Keywords:

Advection–reaction–diffusion

Viscous flow in porous media

Primal-mixed finite element methods

Coupling algorithms

Operator splitting

ABSTRACT

We present a partitioned algorithm aimed at extending the capabilities of existing solvers for the simulation of coupled advection–diffusion–reaction systems and incompressible, viscous flow. The space discretisation of the governing equations is based on mixed finite element methods defined on unstructured meshes, whereas the time integration hinges on an operator splitting strategy that exploits the differences in scales between the reaction, advection, and diffusion processes, considering the global system as a number of sequentially linked sets of partial differential, and algebraic equations. The flow solver presents the advantage that all unknowns in the system (here vorticity, velocity, and pressure) can be fully decoupled and thus turn the overall scheme very attractive from the computational perspective. The robustness of the proposed method is illustrated with a series of numerical tests in 2D and 3D, relevant in the modelling of bacterial bioconvection and Boussinesq systems.

© 2017 Elsevier Inc. All rights reserved.

1. Introduction

Scope Our interest is in the efficient solution of advection–diffusion–reaction (ADR) systems coupled with the equations governing incompressible viscous flow within porous media (namely the Stokes–Darcy, or Brinkman equations). A fairly large class of problems in science and engineering assume such a particular structure, as it is one of the basic forms of representing systems where physical, biological, and chemical processes exhibit a remarkable interaction. Notable examples are the density fingering of exothermic fronts in Hele–Shaw cells [19], where hydrodynamic instabilities are strongly influenced by the chemical reactions taking place at different spatial and temporal scales; convection-driven Turing patterns generated using Schnackenberg–Darcy models [26]; reversible reactive flow and viscous fingering in chromatographic separation [2, 29]; plankton dynamics [25]; forced-convective heat and mass transfer in fibrous porous materials [8]; or the bioconvection in porous suspensions of oxytactic bacteria [17,23]. Phenomena of this kind are also relevant in so-called doubly-diffusive flows [22,28,31], where convective effects are driven by two different density gradients having diverse rates of diffusion.

While the specific nature of the physical system of interest will imply diverse forms of coupling mechanisms, our goal is to focus on the interaction of the building-block systems through mass transport and external flow forces. Moreover, depending on the formulation and complexity of the underlying PDE-based model, the numerical solution of the problem may become a significant computational challenge. In particular, ADR equations feature intrinsic difficulties on their own

* Corresponding author.

E-mail addresses: pietro.lenarda@imtlucca.it (P. Lenarda), marco.paggi@imtlucca.it (M. Paggi), ruizbaier@maths.ox.ac.uk (R. Ruiz Baier).

(related to high nonlinearities, targeting the preservation of physical properties, or stiffness of the ODE systems resulting from space discretisation, cf. [27]), which greatly intensify in the presence of coupling with flow equations, themselves being populated with complications very well-known to the CFD community (including violation of local conservativity, accuracy affected by heterogeneous coefficients, discrete inf-sup conditions, and many others. See e.g. [13,16]). The numerical solution of coupled PDEs via operator splitting techniques has a well-established tradition and many specialised contributions are available (cf. the monograph [18] and its abundant list of references). A few recent works analysing schemes for the partitioned coupling of reaction-diffusion systems and flow equations include, for instance, Runge-Kutta-DG splitting methods for miscible displacement in porous media [24] and conservative finite volume-element schemes for the coupling of flow and transport [10,33]. A similar structure of the coupled equations is shared by other classical systems as the Biot equations in poroelasticity, or thermoelasticity-based problems, for which a much richer, numerically-oriented literature is available (see e.g. [3,9,14,20,21,30,32] and the references therein).

Other contributions closely related to the present work include the discussion on nonlinear stability of doubly-diffusive interactions in Brinkman flows exposed in [1], whereas numerical simulations in the two-dimensional case were performed in [11]. Here we explore very similar scenarios, but allowing the diffusive terms to depend nonlinearly on the species concentrations, we consider the three-dimensional case as well, and we write the Brinkman equations in terms of vorticity, velocity, and pressure of the incompressible fluid. We stress that the mathematical properties of such a formulation have been addressed only recently in [4], where also an explicit finite element method was introduced for its numerical approximation. The present work essentially complements [1,4] in the sense that we define a family of four basic coupling methods to numerically solve the governing equations. The precise form of the schemes will vary depending on whether the Brinkman problem admits a pure vorticity formulation (as the one proposed in [7]), and on two main sequential substructuring techniques to decouple the advection-diffusion from the reaction steps in the ADR system. Insight on the properties of each coupling strategy will be sought via a theoretical *a priori* stability analysis of the separate blocks, whereas the discretisation will then follow the natural formulation adopted by the particular splitting of the problem. For instance, one of the resulting methods consists of Raviart-Thomas approximation of velocity, the discrete vorticity is constructed with Nédélec elements, pressure is approximated with piecewise constant elements, and the species' concentrations with piecewise linear and continuous Lagrange elements. A thorough comparison between the splitting methods will be given in terms of computational burden, experimental accuracy, and behaviour of the nonlinear solvers.

Outline We have structured the contents of this paper in the following way. In Section 2, we summarise the main ingredients of the model problem and introduce its weak formulation. Section 3 considers the finite element discretisation and describes the decoupling mechanisms applied to the fully nonlinear problem, focusing on the flow-ADR interaction, whereas two examples of splitting techniques for the ADR blocks are discussed in Section 4. Numerical simulations are shown and extensively discussed in Section 5, and we close with a few final remarks collected in Section 6.

2. Problem formulation

2.1. The governing equations

The coupled system of interest takes place in a bounded domain $\Omega \subset \mathbb{R}^d$, $d = 2, 3$ with Lipschitz boundary. It can be derived from basic principles of mass, momentum, and energy conservation, and its final form is written in terms of the fluid velocity $\mathbf{u} = (u_1, \dots, u_d)^T$, the rescaled vorticity $\boldsymbol{\omega}$ (vector $(\omega_1, \omega_2, \omega_3)^T$ if $d = 3$, or scalar ω if $d = 2$), the pressure p , and a vector $\mathbf{c} = (c_1, \dots, c_m)^T$ of volumetric fraction or total dissolved concentration of m distinct substances: For a.e. $(\mathbf{x}, t) \in \Omega_T := \Omega \times [0, T]$,

$$\begin{aligned} \partial_t \mathbf{c} + (\mathbf{u} \cdot \nabla) \mathbf{c} - \operatorname{div}(\mathbf{D}(\mathbf{c}) \nabla \mathbf{c}) &= \mathbf{G}(\mathbf{c}), \\ \sigma \mathbf{u} + \sqrt{\mu} \operatorname{curl} \boldsymbol{\omega} + \nabla p &= \rho \mathbf{F}(\mathbf{c}), \\ \boldsymbol{\omega} &= \sqrt{\mu} \operatorname{curl} \mathbf{u}, \\ \operatorname{div} \mathbf{u} &= 0, \end{aligned} \tag{2.1}$$

where ρ, μ are the fluid density and viscosity, respectively (here assumed positive, constant parameters), $\sigma(\mathbf{x})$ is the inverse permeability tensor, \mathbf{F} represents the force exerted by the species on the fluid motion, encoding also external forces, \mathbf{D} is a (generally nonlinear) cross-diffusion matrix, and \mathbf{G} contains the reaction kinetics (representing production and degradation) of the species.

Model (2.1) assumes that changes in the chemical concentrations do not influence thermophysical properties of the fluid such as viscosity or density, but rather they are nonlinearly coupled by the source term on the momentum equation. Conversely, we suppose that the viscous flow affects the species dynamics by means of advection only. The model also considers that the interaction of the species takes place in a porous medium composed of a bed of light fixed particles. Equations (2.1) are complemented with the following standard boundary and initial data:

$$\begin{aligned} (\mathbf{c} \mathbf{u}^T - \mathbf{D}(\mathbf{c}) \nabla \mathbf{c}) \mathbf{n} &= \mathbf{0}, \quad \mathbf{u} \cdot \mathbf{n} = u_\partial, \quad \boldsymbol{\omega} \times \mathbf{n} = \boldsymbol{\omega}_\partial, \quad (\mathbf{x}, t) \in \partial\Omega \times [0, T], \\ \mathbf{c} &= \mathbf{c}_0, \quad (\mathbf{x}, t) \in \Omega \times \{0\}, \end{aligned} \tag{2.2}$$

stating that no flux occurs across the boundary (the species cannot leave the medium), and that a slip velocity together with a compatible vorticity trace are imposed along the domain boundary. These will be assumed homogeneous in the rest of the presentation.

2.2. Weak form under two different Brinkman formulations

We proceed to derive a weak formulation for (2.1). First, let us introduce the trial spaces where the weak solutions will live, and whose natural regularity is indicated by the formulation below: $\mathbf{c} \in L^2(0, T; \mathbf{S})$, $\partial_t \mathbf{c} \in L^2(0, T; \mathbf{S}')$, $\mathbf{u} \in L^2(0, T; \mathbf{V})$, $\omega \in L^1(0, T; \mathbf{W})$, and $p \in L^2(\Omega \times [0, T])$; with $\mathbf{S} := \mathbf{H}^1(\Omega)$, $\mathbf{V} := \mathbf{H}(\text{div}; \Omega)$, $\mathbf{W} := \mathbf{H}(\mathbf{curl}; \Omega)$ and $Q := L_0^2(\Omega) = \{q \in L^2(\Omega) : \int_{\Omega} q = 0\}$.

The ADR equations are multiplied by $\mathbf{s} \in \mathbf{S}_0$ and integrated by parts over the spatial domain, the momentum equation for the flow is tested against $\mathbf{v} \in \mathbf{V}_0$, the constitutive relation is tested against $\theta \in \mathbf{W}_0$, and the mass conservation law is multiplied by $q \in Q$. In turn, the boundary conditions (2.2) suggest the following definition of the test spaces

$$\mathbf{S}_0 = \{\mathbf{s} \in \mathbf{S} : \mathbf{s} = \mathbf{0} \text{ on } \partial\Omega\}, \quad \mathbf{V}_0 = \{\mathbf{v} \in \mathbf{V} : \mathbf{v} \cdot \mathbf{n} = 0 \text{ on } \partial\Omega\}, \quad \mathbf{W}_0 = \{\theta \in \mathbf{W} : \theta \times \mathbf{n} = \mathbf{0} \text{ on } \partial\Omega\},$$

which leads to the problem: For $t \in (0, T]$, find $(\mathbf{c}(t), \mathbf{u}(t), \omega(t), p(t)) \in \mathbf{S} \times \mathbf{V} \times \mathbf{W} \times Q$ such that

$$\begin{aligned} & \int_{\Omega} [\partial_t \mathbf{c}(t) + (\mathbf{u}(t) \cdot \nabla) \mathbf{c}] \cdot \mathbf{s} + \int_{\Omega} \mathbf{D}(\mathbf{c}(t)) \nabla \mathbf{c}(t) : \nabla \mathbf{s} = \int_{\Omega} \mathbf{G}(\mathbf{c}(t)) \cdot \mathbf{s}, \quad \forall \mathbf{s} \in \mathbf{S}_0, \\ & \int_{\Omega} \sigma \mathbf{u}(t) \cdot \mathbf{v} + \sqrt{\mu} \int_{\Omega} \mathbf{curl} \omega(t) \cdot \mathbf{v} - \int_{\Omega} p(t) \operatorname{div} \mathbf{v} = \int_{\Omega} \rho \mathbf{F}(\mathbf{c}(t)) \cdot \mathbf{v}, \quad \forall \theta \in \mathbf{W}_0, \\ & \sqrt{\mu} \int_{\Omega} \mathbf{u}(t) \cdot \mathbf{curl} \theta - \int_{\Omega} \omega(t) \cdot \theta = 0, \quad \forall \mathbf{v} \in \mathbf{V}_0, \\ & - \int_{\Omega} q \operatorname{div} \mathbf{u}(t) = 0, \quad \forall q \in Q. \end{aligned} \tag{2.3}$$

Setting $\chi = (\mathbf{c}, \mathbf{u}, \omega, p)^T$, the matrix form of (2.3) can be recast as follows

$$\begin{pmatrix} \mathcal{A}_{\mathbf{c}} & \mathbf{0} & \mathbf{0} & \mathbf{0} \\ \mathbf{0} & \mathbf{0} & \mathbf{0} & \mathbf{0} \\ \mathbf{0} & \mathbf{0} & \mathbf{0} & \mathbf{0} \\ \mathbf{0} & \mathbf{0} & \mathbf{0} & \mathbf{0} \end{pmatrix} \dot{\chi}(t) + \begin{pmatrix} \mathcal{D} - \mathcal{G}'_1 & \mathcal{C} & \mathbf{0} & \mathbf{0} \\ -\mathcal{F} & \mathcal{A}_{\mathbf{u}} & \mathcal{B}_1 & -\mathcal{B}_2 \\ \mathbf{0} & \mathcal{B}_1^* & -\mathcal{A}_{\omega} & \mathbf{0} \\ \mathbf{0} & -\mathcal{B}_2^* & \mathbf{0} & \mathbf{0} \end{pmatrix} \chi(t) = \mathbf{0}, \tag{2.4}$$

where dashed lines separate sub-blocks associated to the ADR and Brinkman systems, and the linear and nonlinear operators defining the matrix system are given by

$$\begin{aligned} [\mathcal{A}_{\mathbf{c}}(\mathbf{c}), \mathbf{s}] &:= \int_{\Omega} \mathbf{c} \cdot \mathbf{s}, \quad [\mathcal{C}(\mathbf{c}); \mathbf{u}, \mathbf{s}] := \int_{\Omega} (\mathbf{u} \cdot \nabla) \mathbf{c} \cdot \mathbf{s}, \quad [\mathcal{D}(\mathbf{c}), \mathbf{s}] := \int_{\Omega} \mathbf{D}(\mathbf{c}) \nabla \mathbf{c} : \nabla \mathbf{s}, \\ [\mathcal{G}(\mathbf{c}), \mathbf{s}] &:= \int_{\Omega} \mathbf{G}(\mathbf{c}) \cdot \mathbf{s}, \quad [\mathcal{F}(\mathbf{c}), \mathbf{v}] := \int_{\Omega} \rho \mathbf{F}(\mathbf{c}) \cdot \mathbf{v}, \quad [\mathcal{A}_{\mathbf{u}}(\mathbf{u}), \mathbf{v}] := \int_{\Omega} \sigma \mathbf{u} \cdot \mathbf{v}, \\ [\mathcal{B}_1(\omega), \mathbf{v}] &:= \int_{\Omega} \sqrt{\mu} \mathbf{curl} \omega \cdot \mathbf{v}, \quad [\mathcal{B}_2(p), \mathbf{v}] := \int_{\Omega} p \operatorname{div} \mathbf{v}, \quad [\mathcal{A}_{\omega}(\omega), \theta] := \int_{\Omega} \omega \cdot \theta. \end{aligned}$$

Here the diffusion, reaction, and forcing terms are assumed smooth enough: \mathbf{D} is positive, monotone (or coercive in the linear case), and continuous; \mathbf{G} is continuous, uniformly bounded, and positivity preserving; and \mathbf{F} is linear in \mathbf{c} . More precise conditions on the coefficients will be specified later on. Classical derivations of *a priori* stability bounds will require an additional regularity for the velocity $\mathbf{u} \in L^2(0, T; \mathbf{V}) \cap L^\infty(0, T; L^\infty(\Omega)^d)$ (see e.g. [12,15] for flow-transport coupling in the context of miscible displacement in porous media).

Alternatively from (2.3), we can picture a formulation where adequate manipulations of the Brinkman equations allow a decoupling between the velocity, vorticity, and pressure blocks, under the assumption of uniformly bounded permeability and homogeneous boundary conditions for velocity and vorticity (see [7]). The weak form is obtained by testing the constitutive equation in (2.1) against functions in \mathbf{W}_0 , integrating by parts, and writing the velocity in terms of vorticity and pressure using the momentum equation in (2.1). Then, after applying again an integration by parts, one can eventually reformulate (2.4) as

$$\begin{pmatrix} \mathcal{A}_c & \mathbf{0} & \mathbf{0} & \mathbf{0} \\ \mathbf{0} & \mathbf{0} & \mathbf{0} & \mathbf{0} \\ \mathbf{0} & \mathbf{0} & \mathbf{0} & \mathbf{0} \\ \mathbf{0} & \mathbf{0} & \mathbf{0} & \mathbf{0} \end{pmatrix} \dot{\chi}(t) + \begin{pmatrix} \mathcal{D} - \mathcal{G}^T & \mathcal{C} & \mathbf{0} & \mathbf{0} \\ -\mathcal{F}_1 & \mathcal{A}_u & \mathbf{0} & \mathbf{0} \\ -\mathcal{F}_2 & \mathbf{0} & -\widehat{\mathcal{A}}_\omega & \mathbf{0} \\ -\mathcal{F}_3 & \mathbf{0} & \mathbf{0} & \widehat{\mathcal{A}}_p \end{pmatrix} \chi(t) = \mathbf{0}, \quad (2.5)$$

where the modified blocks read

$$[\widehat{\mathcal{A}}_\omega(\boldsymbol{\omega}, \theta)] := \int_{\Omega} \sigma \boldsymbol{\omega} \cdot \theta + \int_{\Omega} \mu \operatorname{curl} \boldsymbol{\omega} \cdot \operatorname{curl} \theta, \quad [\mathcal{F}_2(\mathbf{c}, \theta)] := \int_{\Omega} \sqrt{\mu} \rho \mathbf{F}(\mathbf{c}) \cdot \operatorname{curl} \theta,$$

$$[\widehat{\mathcal{A}}_p(p, q)] := \int_{\Omega} \nabla p \cdot \nabla q, \quad [\mathcal{F}_3(\mathbf{c}), q] := \int_{\Omega} \rho \mathbf{F}(\mathbf{c}) \cdot \nabla q,$$

$$[\mathcal{F}_1(\mathbf{c}), \mathbf{v}] := \int_{\Omega} (\rho \mathbf{F}(\mathbf{c}) - \sqrt{\mu} \operatorname{curl} \tilde{\boldsymbol{\omega}} - \nabla \tilde{p}) \cdot \mathbf{v},$$

and where $\tilde{\cdot}$ denotes an *uncoupled* quantity. Another crucial difference with respect to (2.3), is that the pressure requires higher regularity (now $Q = H^1(\Omega) \cap L_0^2(\Omega)$), and that the velocity is only needed in $L^2(0, T; L^2(\Omega)) \cap L^\infty(0, T; L^\infty(\Omega)^d)$. Both Brinkman formulations lead to symmetric systems, which is a property that may be exploited by specialised preconditioners and iterative solvers.

2.3. A general operator splitting

Using the matrix systems (2.4) and (2.5), one can readily state a general splitting of the coupled ADR-Brinkman problem in the form

$$\mathcal{H}_0 \dot{\chi} + \mathcal{H}_1 \chi + \mathcal{H}_2 \chi = \mathbf{0},$$

where the operators \mathcal{H}_i , $i = 0, 1, 2$ are formally defined by

$$\mathcal{H}_0 = \begin{pmatrix} \mathcal{A}_c & \mathbf{0} & \cdots \\ \mathbf{0} & \mathbf{0} & \cdots \\ \vdots & \vdots & \ddots \end{pmatrix}, \quad \mathcal{H}_1 = \begin{pmatrix} \mathcal{D} - \mathcal{G} + \mathcal{C} & \mathbf{0} & \cdots \\ \mathbf{0} & \mathbf{0} & \cdots \\ \vdots & \vdots & \ddots \end{pmatrix}, \quad \mathcal{H}_2 = \begin{pmatrix} \mathbf{0} & \mathbf{0} & \mathbf{0} & \mathbf{0} \\ -\mathcal{F} & \mathcal{A}_u & \mathcal{B}_1 & -\mathcal{B}_2 \\ \mathbf{0} & \mathcal{B}_1^* & -\mathcal{A}_\omega & \mathbf{0} \\ \mathbf{0} & -\mathcal{B}_2^* & \mathbf{0} & \mathbf{0} \end{pmatrix},$$

if using (2.4), or assuming the modified form

$$\mathcal{H}_2 = \begin{pmatrix} \mathbf{0} & \mathbf{0} & \mathbf{0} & \mathbf{0} \\ -\mathcal{F}_1 & \mathcal{A}_u & \mathbf{0} & \mathbf{0} \\ -\mathcal{F}_2 & \mathbf{0} & -\widehat{\mathcal{A}}_\omega & \mathbf{0} \\ -\mathcal{F}_3 & \mathbf{0} & \mathbf{0} & \widehat{\mathcal{A}}_p \end{pmatrix},$$

if using (2.5). Then, the solution of the ADR system can be characterised by $\mathcal{H}_0 \dot{\chi} + \mathcal{H}_1 \chi = \mathbf{0}$, and that of the Brinkman blocks by $\mathcal{H}_2 \chi = \mathbf{0}$.

In turn, and as will be specified later in Section 4, the solution of the ADR system can be split again into a pure advection-diffusion and a pure reaction step, $\mathcal{H}_0 \dot{\chi} + \mathcal{H}_{11} \chi = \mathbf{0}$ and $\mathcal{H}_0 \dot{\chi} + \mathcal{H}_{12} \chi = \mathbf{0}$, respectively, where

$$\mathcal{H}_{11} = \begin{pmatrix} \mathcal{D} + \mathcal{C} & \mathbf{0} & \cdots \\ \mathbf{0} & \mathbf{0} & \cdots \\ \vdots & \vdots & \ddots \end{pmatrix}, \quad \mathcal{H}_{12} = \begin{pmatrix} -\mathcal{G} & \mathbf{0} & \cdots \\ \mathbf{0} & \mathbf{0} & \cdots \\ \vdots & \vdots & \ddots \end{pmatrix}.$$

3. A family of segregated finite element methods

3.1. Meshes and finite dimensional spaces

Let \mathcal{T}_h denote a simplicial decomposition of the spatial domain Ω into elements K of maximum size h . For a fixed $h > 0$ we introduce finite dimensional subspaces for the k -th order approximation of the unknowns: $\mathbf{S}_h \subset \mathbf{S}$, $\mathbf{V}_h \subset \mathbf{V}$, $\mathbf{W}_h \subset \mathbf{W}$, and $Q_h \subset Q$. The concentration and vorticity finite element spaces assume the form

$$\mathbf{S}_h = \{\mathbf{s}_h \in \mathbf{S} : \mathbf{s}_h|_K \in [\mathbb{P}_{k+1}]^m(K), \forall K \in \mathcal{T}_h\}, \quad \mathbf{W}_h = \{\boldsymbol{\theta}_h \in \mathbf{W} : \boldsymbol{\theta}_h|_K \in \mathbb{N}\mathbb{D}_{k+1}(K), \forall K \in \mathcal{T}_h\},$$

while, depending on whether the formulation (2.4) or (2.5) are used, the finite element spaces for the velocity and pressure unknowns are defined as:

$$\mathbf{V}_h = \{\mathbf{v}_h \in \mathbf{V} : \mathbf{v}_h|_K \in \mathbb{RT}_k(K), \forall K \in \mathcal{T}_h\}, \quad Q_h = \{q_h \in L^2(\Omega) : q_h|_K \in \mathbb{P}_k(K), \forall K \in \mathcal{T}_h\},$$

or

$$\mathbf{V}_h = \{\mathbf{v}_h \in \mathbf{V} : \mathbf{v}_h|_K \in [\mathbb{P}_k(K)]^d, \forall K \in \mathcal{T}_h\}, \quad Q_h = \{q_h \in H^1(\Omega) : q_h|_K \in \mathbb{P}_{k+1}(K), \forall K \in \mathcal{T}_h\},$$

respectively. Here \mathbb{RT}_k stands for the local Raviart–Thomas elements of order k ($\mathbf{H}(\text{div}; \Omega)$ -conforming), \mathbb{ND}_k is the local Nédélec vectorial element of degree k ($\mathbf{H}(\mathbf{curl}; \Omega)$ -conforming), and \mathbb{P}_k is the local space of Lagrange finite elements of order k . Spaces \mathbf{S}_h and \mathbf{W}_h are equipped with the following norms as in [7]:

$$\begin{aligned} \|\mathbf{s}_h\|_{\mathbf{H}^1(\Omega)}^2 &:= \|\mathbf{s}_h\|_{L^2(\Omega)}^2 + \|\nabla \mathbf{s}_h\|_{L^2(\Omega)}^2, \quad \forall \mathbf{s}_h \in \mathbf{S}_h, \\ \|\boldsymbol{\theta}_h\|_{1,\mu}^2 &:= \|\boldsymbol{\theta}_h\|_{L^2(\Omega)}^2 + \mu \|\mathbf{curl} \boldsymbol{\theta}_h\|_{L^2(\Omega)}^2, \quad \forall \boldsymbol{\theta}_h \in \mathbf{W}_h. \end{aligned}$$

Notice that the vorticity norm is μ -dependent, and the norms for the spaces \mathbf{V}_h and Q_h defined by the first Brinkman formulation (2.4) are:

$$\|\mathbf{v}_h\|_{\mathbf{H}(\text{div}; \Omega)}^2 := \|\mathbf{v}_h\|_{L^2(\Omega)}^2 + \|\text{div } \mathbf{v}_h\|_{L^2(\Omega)}^2, \quad \forall \mathbf{v}_h \in \mathbf{V}_h,$$

and the natural $L^2(\Omega)$ -norm for Q_h . On the other hand, for the second set of Brinkman equations (2.5) we consider the usual $L^2(\Omega)$ - and $H^1(\Omega)$ -norms for the spaces \mathbf{V}_h and Q_h , respectively.

The Galerkin method associated to (2.4) or (2.5) is presented in what follows, using a partitioned solution approach.

3.2. Outer ADR-Brinkman splitting scheme

A straightforward splitting method consists in, starting from the initial concentrations' distribution, solving the flow equations and then pass the computed velocity to advect the ADR system. For a backward Euler time advancing scheme, and depending on which of the two Brinkman solvers is considered (i.e., using (2.4) or (2.5)), the following steps are applied at each time step t^{n+1} , where the spaces are chosen accordingly to the distinction made in the previous section.

(B1): Given \mathbf{c}_h^n , find $(\mathbf{u}_h^{n+1}, \boldsymbol{\omega}_h^{n+1}, p_h^{n+1}) \in \mathbf{V}_h \times \mathbf{W}_h \times Q_h$ such that:

$$\begin{aligned} \int_{\Omega} \sigma \mathbf{u}_h^{n+1} \cdot \mathbf{v}_h + \sqrt{\mu} \int_{\Omega} \mathbf{curl} \boldsymbol{\omega}_h^{n+1} \cdot \mathbf{v}_h - \int_{\Omega} p_h^{n+1} \text{div } \mathbf{v}_h &= \int_{\Omega} \rho \mathbf{F}(\mathbf{c}_h^n) \cdot \mathbf{v}_h, \quad \forall \mathbf{v}_h \in \mathbf{V}_{h,0}, \\ \sqrt{\mu} \int_{\Omega} \mathbf{u}_h^{n+1} \cdot \mathbf{curl} \boldsymbol{\theta}_h - \int_{\Omega} \boldsymbol{\omega}_h^{n+1} \cdot \boldsymbol{\theta}_h &= 0, \quad \forall \boldsymbol{\theta}_h \in \mathbf{W}_{h,0}, \\ - \int_{\Omega} q_h \text{div } \mathbf{u}_h^{n+1} &= 0, \quad \forall q_h \in Q_{h,0}, \end{aligned} \tag{3.1}$$

or

(B2): Given \mathbf{c}_h^n

– First solve the pure vorticity problem: Find $\boldsymbol{\omega}_h^{n+1} \in \mathbf{W}_h$ such that:

$$\int_{\Omega} \sigma \boldsymbol{\omega}_h^{n+1} \cdot \boldsymbol{\theta}_h + \mu \int_{\Omega} \mathbf{curl} \boldsymbol{\omega}_h^{n+1} \cdot \boldsymbol{\theta}_h = \sqrt{\mu} \int_{\Omega} \rho \mathbf{F}(\mathbf{c}_h^n) \cdot \mathbf{curl} \boldsymbol{\theta}_h, \quad \forall \boldsymbol{\theta}_h \in \mathbf{W}_{h,0}$$

– Then, solve the pure pressure problem:

$$\int_{\Omega} \nabla p_h^{n+1} \cdot \nabla q_h = \int_{\Omega} \rho \mathbf{F}(\mathbf{c}_h^n) \cdot \nabla q_h, \quad \forall Q_h$$

– Finally recover the velocity vector $\mathbf{u}_h^{n+1} \in \mathbf{V}_h$ as:

$$\mathbf{u}_h^{n+1} = \sigma^{-1} \left(\rho \mathbf{F}(\mathbf{c}_h^n) - \sqrt{\mu} \mathbf{curl} \boldsymbol{\omega}_h^{n+1} - \nabla p_h^{n+1} \right).$$

(ADR): Given \mathbf{u}_h^{n+1} solution of the Brinkman problem through (B1) or (B2), solve the ADR problem: find $\mathbf{c}_h^{n+1} \in \mathbf{S}_h$ such that:

$$\int_{\Omega} \frac{\mathbf{c}_h^{n+1} - \mathbf{c}_h^n}{\Delta t} \cdot \mathbf{s}_h + \int_{\Omega} (\mathbf{u}_h^{n+1} \cdot \nabla) \mathbf{c}_h^{n+1} \cdot \mathbf{s}_h + \int_{\Omega} \mathbf{D}(\mathbf{c}_h^{n+1}) \nabla \mathbf{c}_h^{n+1} : \nabla \mathbf{s}_h = \int_{\Omega} \mathbf{G}(\mathbf{c}_h^{n+1}) \cdot \mathbf{s}_h \quad \forall \mathbf{s}_h \in \mathbf{S}_{0,h}. \tag{3.2}$$

The two solution strategies adopting either (B1) or (B2) lead to outer schemes for the Brinkman-ADR problem of the type (B1-ADR) or (B2-ADR). We stress that, for the latter scheme, if lowest order elements are employed (that is, $k = 0$) then an intermediate step is required to ensure that the discrete advective term is well-defined. A projection of \mathbf{u}_h^{n+1} onto \mathbb{RT}_k would typically suffice. The inner solvers for the ADR equations will be made precise in the sequel.

Under suitable hypotheses one can derive the unique solvability of each discrete problem (B1), (B2) and (ADR). More specifically, if $\mathbf{F}(\mathbf{c}_h^n) \in \mathbf{L}^2(\Omega)$ then the invertibility of the discrete Brinkman problem (B1) follows from a discrete inf-sup condition and the Babuška-Brezzi theory [5, Theorem 3.2 & Corollary 3.1]. Likewise, also for $\mathbf{F}(\mathbf{c}_h^n) \in \mathbf{L}^2(\Omega)$, the well-posedness of (B2) is a direct consequence of the Lax-Milgram lemma (see [7, Theorems 3.1 and 3.2] and also [6] for the axisymmetric case). Finally, thanks to the uniform positivity and monotonicity of the operator $\mathbf{D}(\cdot)$, the solvability of the nonlinear discrete problem (ADR) is ensured according to the classical results collected in [12,15] (see also [4]).

Note that while the flow problem is linear, the set of nonlinear ADR equations uses a nested Newton-Raphson iterative scheme to find an approximation of \mathbf{c}_h^{n+1} at each time step.

3.3. A priori estimates for the energy of the system

Let us recall the discrete Gronwall inequality

Lemma 3.1. If $\phi_0 \leq g_0$ and

$$\phi_n \leq g_0 + \sum_{k=0}^{n-1} p_k + \sum_{k=0}^{n-1} q_k \phi_k, \quad \forall n \geq 1,$$

then

$$\phi_n \leq \left(g_0 + \sum_{k=0}^{n-1} p_k \right) \exp \left(\sum_{k=0}^{n-1} q_k \right), \quad \forall n \geq 1.$$

The stability of the outer splitting method described in Section 3.2 is established by the following *a priori* bound, written in terms of the system's discrete energy norm

$$\|\boldsymbol{\chi}_h^n\|^2 := \|\mathbf{u}_h^n\|_{\mathbf{H}(\text{div}; \Omega)}^2 + \|\boldsymbol{\omega}_h^n\|_{1,\mu}^2 + \|p_h^n\|_{L^2(\Omega)}^2 + \|\mathbf{c}_h^n\|_{\mathbf{L}^2(\Omega)}^2, \quad \forall n \geq 0.$$

Before stating the main result in this Section, we recall the following auxiliary *a priori* estimate, to be exploited in the sequel.

Lemma 3.2. Let $\mathbf{c}_h^n \in \mathbf{S}_h$ and assume that $\mathbf{F}(\mathbf{c}) = (\boldsymbol{\alpha} \cdot \mathbf{c})\mathbf{g}$, for constant $\boldsymbol{\alpha} \in \mathbb{R}^m$ and $\mathbf{g} = -\mathbf{e}_3$. Then, the solution $(\mathbf{u}_h^n, \boldsymbol{\omega}_h^n, p_h^n) \in \mathbf{V}_h \times \mathbf{W}_h \times Q_h$ of (3.1) exists and is unique. Moreover, there exists $C > 0$ independent of μ such that:

$$\|p_h\|_{L^2(\Omega)} \leq C \rho \|\mathbf{F}(\mathbf{c}_h^n)\|_{\mathbf{L}^2(\Omega)} = C \rho \|\boldsymbol{\alpha}\| \|\mathbf{c}_h^n\|_{\mathbf{L}^2(\Omega)}.$$

The proof of this result can be found in [5] and it is a consequence of the inf-sup condition satisfied by the bilinear form defined by $[\mathcal{B}_2(p), \mathbf{v}]$.

Theorem 3.3. Let $\boldsymbol{\chi}_h^n = (\mathbf{c}_h^n, \mathbf{u}_h^n, \boldsymbol{\omega}_h^n, p_h^n)$, $\forall n = 0, \dots, N_T$ be the solution of the outer splitting defined by (3.1)–(3.2) in (B1-ADR). Suppose that $\mathbf{F}(\mathbf{c}) = (\boldsymbol{\alpha} \cdot \mathbf{c})\mathbf{g}$, for constant $\boldsymbol{\alpha} \in \mathbb{R}^m$ and $\mathbf{g} = -\mathbf{e}_3$, and assume that there exists $D_{\min} > 0$ such that $\mathbf{s}^T(\mathbf{D}(\mathbf{s})\mathbf{s}) \geq D_{\min} \|\mathbf{s}\|^2$ for all \mathbf{s} . Then, there exist a constant $C(\sigma, \rho, \boldsymbol{\alpha}) > 0$ and positive non-decreasing functions $C_0(t^{n+1}), C_1(t^{n+1})$, such that, for each time step t^n :

$$\|\boldsymbol{\chi}_h^{n+1}\|^2 + 2\Delta t D_{\min}^2 \sum_{k=0}^n \|\nabla \mathbf{c}_h^{k+1}\|_{\mathbf{L}^2(\Omega)}^2 \leq C_0(t^{n+1}) \|\mathbf{c}_h^0\|_{\mathbf{L}^2(\Omega)}^2 + C_1(t^{n+1}) \sum_{k=0}^n \|\mathbf{G}(\mathbf{c}_h^{k+1})\|_{\mathbf{L}^2(\Omega)}^2 + C(\sigma, \rho, \boldsymbol{\alpha}) \|\mathbf{c}_h^n\|_{\mathbf{L}^2(\Omega)}^2.$$

In particular, if $\|\mathbf{G}(\mathbf{c})\|_{\mathbf{L}^2(\Omega)} \leq G$ for a given $G \geq 0$, then, at each timestep the energy norm admits the following bound

$$\|\boldsymbol{\chi}_h^n\|^2 \leq \|\boldsymbol{\chi}_h^0\|^2 \sum_{k=0}^{N_T} C^k(\sigma, \rho, \boldsymbol{\alpha}) C_0(t^{N_T-k}) + G^2 \sum_{k=0}^{N_T} C^k(\sigma, \rho, \boldsymbol{\alpha}) (N_T - k) C_1(t^{N_T-k}) + C^{N_T}(\sigma, \rho, \boldsymbol{\alpha}) \|\boldsymbol{\chi}_h^0\|^2.$$

Proof. Using integration by parts we observe that the convective term in (3.2) can be rewritten in the skew-symmetric form:

$$\int_{\Omega} (\mathbf{u}_h^{n+1} \cdot \nabla) \mathbf{c}_h^{n+1} \cdot \mathbf{s}_h = \frac{1}{2} \int_{\Omega} (\mathbf{u}_h^{n+1} \cdot \nabla) \mathbf{c}_h^{n+1} \cdot \mathbf{s}_h - \frac{1}{2} \int_{\Omega} (\mathbf{u}_h^{n+1} \cdot \nabla) \mathbf{s}_h \cdot \mathbf{c}_h^{n+1}.$$

Next, testing equation (3.2) with $\mathbf{s}_h = \mathbf{c}_h^{n+1} \in \mathbf{S}_h$ and using Young's inequality we have:

$$\begin{aligned} & \frac{1}{2} \|\mathbf{c}_h^{n+1}\|_{\mathbf{L}^2(\Omega)}^2 + \Delta t D_{\min} \|\nabla \mathbf{c}_h^{n+1}\|_{\mathbf{L}^2(\Omega)}^2 \\ & \leq \frac{1}{2} \|\mathbf{c}_h^n\|_{\mathbf{L}^2(\Omega)}^2 + \frac{\Delta t}{2} \|\mathbf{G}(\mathbf{c}_h^{n+1})\|_{\mathbf{L}^2(\Omega)}^2 + \frac{\Delta t}{2} \|\mathbf{c}_h^{n+1}\|_{\mathbf{L}^2(\Omega)}^2, \end{aligned}$$

and summing up for $k = 0, \dots, n-1$ implies that

$$\begin{aligned} & \frac{1}{2} \|\mathbf{c}_h^n\|_{\mathbf{L}^2(\Omega)}^2 + \Delta t D_{\min} \sum_{k=0}^{n-1} \|\nabla \mathbf{c}_h^{k+1}\|_{\mathbf{L}^2(\Omega)}^2 \\ & \leq \frac{1}{2} \|\mathbf{c}_h^0\|_{\mathbf{L}^2(\Omega)}^2 + \frac{\Delta t}{2} \sum_{k=0}^{n-1} \|\mathbf{G}(\mathbf{c}_h^{k+1})\|_{\mathbf{L}^2(\Omega)}^2 + \frac{\Delta t}{2} \sum_{k=0}^{n-1} \|\mathbf{c}_h^{k+1}\|_{\mathbf{L}^2(\Omega)}^2. \end{aligned} \quad (3.3)$$

Applying Lemma 3.1 we can then write:

$$\|\mathbf{c}_h^n\|_{\mathbf{L}^2(\Omega)}^2 \leq \exp(t^n) \left\{ \|\mathbf{c}_h^0\|_{\mathbf{L}^2(\Omega)}^2 + \Delta t \sum_{k=0}^{n-1} \|\mathbf{G}(\mathbf{c}_h^{k+1})\|_{\mathbf{L}^2(\Omega)}^2 \right\}, \quad \forall n \geq 1.$$

Applying this reasoning for $n+1$, and substituting back in the last term of (3.3), after collecting terms we obtain that there are two functions $C_0(t^{n+1}), C_1(t^{n+1}) > 0$ such that the following estimate holds:

$$\|\mathbf{c}_h^{n+1}\|_{\mathbf{L}^2(\Omega)}^2 + 2\Delta t D_{\min} \sum_{k=0}^n \|\nabla \mathbf{c}_h^{k+1}\|_{\mathbf{L}^2(\Omega)}^2 \leq C_0(t^{n+1}) \|\mathbf{c}_h^0\|_{\mathbf{L}^2(\Omega)}^2 + C_1(t^{n+1}) \sum_{k=0}^n \|\mathbf{G}(\mathbf{c}_h^{k+1})\|_{\mathbf{L}^2(\Omega)}^2. \quad (3.4)$$

On the other hand, regarding the Brinkman problem, we proceed to test (3.1) against

$$\mathbf{v}_h = \mathbf{u}_h^{n+1} + c_1 \sqrt{\mu} \operatorname{curl} \boldsymbol{\omega}_h^{n+1} \in \mathbf{V}_{0,h}, \quad \boldsymbol{\theta}_h = -\boldsymbol{\omega}_h^{n+1} \in \mathbf{W}_{0,h}, \quad q_h = -p_h^{n+1} - c_2 \operatorname{div} \mathbf{u}_h^{n+1} \in Q_h,$$

where c_1 and c_2 are positive constants to be determined. Summing up in (3.1) we have:

$$\begin{aligned} & \sigma \|\mathbf{u}_h^{n+1}\|_{\mathbf{L}^2(\Omega)}^2 + \int_{\Omega} \sigma c_1 \sqrt{\mu} \mathbf{u}_h^{n+1} \cdot \operatorname{curl} \boldsymbol{\omega}_h^{n+1} + \int_{\Omega} \sqrt{\mu} \operatorname{curl} \boldsymbol{\omega}_h^{n+1} \cdot \mathbf{u}_h^{n+1} + c_1 \mu \|\operatorname{curl} \boldsymbol{\omega}_h^{n+1}\|_{\mathbf{L}^2(\Omega)}^2 \\ & - \int_{\Omega} p_h^{n+1} \operatorname{div} \mathbf{u}_h^{n+1} - \int_{\Omega} p_h^{n+1} c_1 \sqrt{\mu} \operatorname{div} \operatorname{curl} \boldsymbol{\omega}_h^{n+1} - \int_{\Omega} \sqrt{\mu} \mathbf{u}_h^{n+1} \cdot \operatorname{curl} \boldsymbol{\omega}_h^{n+1} \\ & + \|\boldsymbol{\omega}_h^{n+1}\|_{\mathbf{L}^2(\Omega)}^2 + \int_{\Omega} p_h^{n+1} \operatorname{div} \mathbf{u}_h^{n+1} + c_2 \|\operatorname{div} \mathbf{u}_h^{n+1}\|_{\mathbf{L}^2(\Omega)}^2 \\ & = \int_{\Omega} \rho \mathbf{F}(\mathbf{c}_h^n) \cdot \mathbf{u}_h^{n+1} + \int_{\Omega} c_1 \sqrt{\mu} \rho \mathbf{F}(\mathbf{c}_h^n) \cdot \operatorname{curl} \boldsymbol{\omega}_h^{n+1}, \end{aligned}$$

and then applying Young's inequality gives:

$$\begin{aligned} & c_1 \sqrt{\mu} \int_{\Omega} \sigma \mathbf{u}_h^{n+1} \cdot \operatorname{curl} \boldsymbol{\omega}_h^{n+1} \geq -\frac{\sigma_{\min}}{2} \|\mathbf{u}_h^{n+1}\|_{\mathbf{L}^2(\Omega)}^2 - \frac{c_1^2 \sigma_{\max}^2}{2 \sigma_{\min}} \mu \|\operatorname{curl} \boldsymbol{\omega}_h^{n+1}\|_{\mathbf{L}^2(\Omega)}^2, \\ & \int_{\Omega} \rho \mathbf{F}(\mathbf{c}_h^{n+1}) \cdot \mathbf{u}_h^{n+1} \leq \frac{\sigma_{\min}}{4} \|\mathbf{u}_h^{n+1}\|_{\mathbf{L}^2(\Omega)}^2 + \frac{\rho^2}{\sigma_{\min}} \|\boldsymbol{\alpha}\|^2 \|\mathbf{c}_h^n\|_{\mathbf{L}^2(\Omega)}^2, \\ & \int_{\Omega} c_1 \sqrt{\mu} \rho \mathbf{F}(\mathbf{c}_h^n) \cdot \operatorname{curl} \boldsymbol{\omega}_h^{n+1} \leq \frac{c_1^2 \mu}{2} \|\operatorname{curl} \boldsymbol{\omega}_h^{n+1}\|_{\mathbf{L}^2(\Omega)}^2 + \frac{\rho^2}{2} \|\boldsymbol{\alpha}\|^2 \|\mathbf{c}_h^n\|_{\mathbf{L}^2(\Omega)}^2. \end{aligned}$$

Because $\operatorname{div} \operatorname{curl}$ is the zero operator, we have that $\mathbf{F}(\mathbf{c}_h^n) = (\boldsymbol{\alpha} \cdot \mathbf{c}_h^n) \mathbf{g}$, and collecting terms we obtain:

$$\begin{aligned} \frac{\sigma_{\min}}{4} \|\boldsymbol{u}_h^{n+1}\|_{\mathbf{L}^2(\Omega)}^2 + c_2 \|\operatorname{div} \boldsymbol{u}_h^{n+1}\|_{\mathbf{L}^2(\Omega)}^2 + c_1 \left\{ 1 - \frac{c_1}{2} \left(\frac{\sigma_{\max}^2}{\sigma_{\min}} + 1 \right) \right\} \mu \|\operatorname{curl} \boldsymbol{\omega}_h^{n+1}\|_{\mathbf{L}^2(\Omega)}^2 + \|\boldsymbol{\omega}_h^{n+1}\|_{\mathbf{L}^2(\Omega)}^2 \\ \leq \rho^2 \|\boldsymbol{\alpha}\|^2 \left(\frac{1}{\sigma_{\min}} + \frac{1}{2} \right) \|\boldsymbol{c}_h^n\|_{\mathbf{L}^2(\Omega)}^2. \end{aligned}$$

Notice that the term involving the norm of pressure has disappeared. Taking $c_1 = \frac{\sigma_{\min}}{(\sigma_{\max}^2 + \sigma_{\min})}$, $c_2 = \frac{\sigma_{\min}}{4}$ we obtain that there exists a constant $\tilde{C}(\sigma, \rho, \boldsymbol{\alpha}) > 0$ such that:

$$\|\boldsymbol{u}_h^{n+1}\|_{\mathbf{L}^2(\Omega)}^2 + \|\operatorname{div} \boldsymbol{u}_h^{n+1}\|_{\mathbf{L}^2(\Omega)}^2 + \|\boldsymbol{\omega}_h^{n+1}\|_{\mathbf{L}^2(\Omega)}^2 + \mu \|\operatorname{curl} \boldsymbol{\omega}_h^{n+1}\|_{\mathbf{L}^2(\Omega)}^2 \leq \tilde{C}(\sigma, \rho, \boldsymbol{\alpha}) \|\boldsymbol{c}_h^n\|_{\mathbf{L}^2(\Omega)}^2.$$

The next step consists in recovering an estimate for the norm of the solution of the Brinkman problem involving the pressure norm. This is done via [Lemma 3.2](#), from which we obtain that there is a constant $C(\sigma, \rho, \boldsymbol{\alpha}) > 0$ such that:

$$\|\boldsymbol{u}_h^n\|_{\mathbf{H}(\operatorname{div}, \Omega)}^2 + \|\boldsymbol{\omega}_h^n\|_{1,\mu}^2 + \|p_h^n\|_{L^2(\Omega)}^2 \leq C(\sigma, \rho, \boldsymbol{\alpha}) \|\boldsymbol{c}_h^n\|_{\mathbf{L}^2(\Omega)}^2. \quad (3.5)$$

Combining estimates (3.4) and (3.5) we have the desired result. \square

4. Dedicated partitioned schemes for the ADR equations

We now address the numerical solution of the nonlinear ADR problem (3.2). Based on the structure of the nonlinear diffusion matrix $\mathbf{D}(\mathbf{c})$ and of the reaction vector $\mathbf{G}(\mathbf{c}) = (G_1(\mathbf{c}), \dots, G_m(\mathbf{c}))$, diverse techniques can be employed. Let $\{\boldsymbol{\varphi}_i : i = 1, \dots, N_{\mathbf{S}_h}\}$ be the vector-valued basis of shape functions of the finite element space for the concentration \mathbf{S}_h , where $N_{\mathbf{S}_h} = \dim(\mathbf{S}_h)$. Then we denote the finite element approximation of the concentration vector as:

$$\mathbf{c}_h(\mathbf{x}, t^n) = \sum_{i=1}^{N_{\mathbf{S}_h}} \mathbf{C}_i(t^n) \boldsymbol{\varphi}_i(\mathbf{x}) = \sum_{i=1}^{N_{\mathbf{S}_h}} \sum_{j=1}^m C_i^j(t^n) \boldsymbol{\varphi}_i^j(\mathbf{x}), \quad (4.1)$$

where $M_{\mathbf{S}_h} = \frac{N_{\mathbf{S}_h}}{m}$ and C_i^j represents the j -th component of \mathbf{c}_h at the mesh node i and we regrouped the basis vectors as $\boldsymbol{\varphi}_i^1 = (\varphi_i, \dots, 0)^T, \dots, \boldsymbol{\varphi}_i^m = (0, \dots, \varphi_i)^T$.

The algebraic form of (3.2) is derived by substituting in the weak formulation the expression (4.1) and the analogous form for the test function. First we will focus on a monolithic solver for the ADR system based on a Newton method with full Jacobian.

4.1. A fully implicit Newton–Raphson method

From (3.2) the following nonlinear algebraic system must be solved at each time-step t^{n+1} :

$$\left(\frac{A_{\mathbf{c}}}{\Delta t} + C(\mathbf{u}_h^{n+1}) + D(\mathbf{C}^{n+1}) \right) \mathbf{C}^{n+1} = \tilde{\mathbf{G}}(\mathbf{C}^{n+1}) + \frac{1}{\Delta t} \mathbf{C}^n, \quad (4.2)$$

where the global nodal concentration vector in $\mathbb{R}^{N_{\mathbf{S}_h}}$ and the reaction vector are:

$$(\mathbf{C}^n)_i = \mathbf{C}_i^n, \quad (\tilde{\mathbf{G}}(\mathbf{C}))_i = \int_{\Omega} \mathbf{G} \left(\sum_{k=1}^{N_{\mathbf{S}_h}} \mathbf{C}_k \boldsymbol{\varphi}_k \right) \boldsymbol{\varphi}_i, \quad i = 1, \dots, N_{\mathbf{S}_h}, \quad (4.3)$$

and matrices $A_{\mathbf{c}}$, C , D in $\mathbb{R}^{N_{\mathbf{S}_h} \times \mathbb{R}^{N_{\mathbf{S}_h}}}$ are given by:

$$\begin{aligned} (A_{\mathbf{c}})_{ij} &= \int_{\Omega} \boldsymbol{\varphi}_j \cdot \boldsymbol{\varphi}_i, \quad (C)_{ij} = \int_{\Omega} (\mathbf{u}_h^{n+1} \cdot \nabla) \boldsymbol{\varphi}_j \cdot \boldsymbol{\varphi}_i, \\ (D(\mathbf{C}))_{ij} &= \int_{\Omega} \mathbf{D} \left(\sum_{k=1}^{N_{\mathbf{S}_h}} \mathbf{C}_k \boldsymbol{\varphi}_k \right) \nabla \boldsymbol{\varphi}_j : \nabla \boldsymbol{\varphi}_i. \end{aligned} \quad (4.4)$$

Notice that the convection matrix C depends on the velocity vector \mathbf{u}_h^{n+1} , solution of the Brinkman problem computed at the previous stage of the splitting scheme so that it is constant with respect to the unknown concentration vector \mathbf{c}_h^{n+1} . The nonlinearity of system (4.2) resides in the diffusion matrix D and in the reaction vector $\tilde{\mathbf{G}}$ which are functions of the unknown vector \mathbf{c}_h^{n+1} . We introduce the monolithic ADR residual vector:

$$\mathbf{R}^n(\mathbf{C}) := \left(\frac{A_{\mathbf{c}}}{\Delta t} + C(\mathbf{u}_h^{n+1}) + D(\mathbf{C}) \right) \mathbf{C} - \tilde{\mathbf{G}}(\mathbf{C}) - \frac{A_{\mathbf{c}}}{\Delta t} \mathbf{C}^n,$$

and realise that solving (4.2) is equivalent to solve $\mathbf{R}^n(\mathbf{C}^{n+1}) = \mathbf{0}$. With this purpose, we employ the Newton–Raphson iterative procedure: Suppose that at time t^n and k -th iteration of the Newton–Raphson method, we are given an approximation $\mathbf{C}^{n+1,k}$ of the concentration vector \mathbf{C}^{n+1} , then we solve the following linear system in the correction $\delta\mathbf{C}$ and update as:

$$\left(\frac{A_{\mathbf{c}}}{\Delta t} + C(\mathbf{u}_h^{n+1}) + \tilde{D}(\mathbf{C}^{n+1,k}) - \frac{\partial \tilde{\mathbf{G}}}{\partial \mathbf{C}}(\mathbf{C}^{n+1,k}) \right) \delta\mathbf{C} = -\mathbf{R}^n(\mathbf{C}^{n+1,k}), \quad (4.5)$$

$$\mathbf{C}^{n+1,k+1} = \mathbf{C}^{n+1,k} + \delta\mathbf{C}, \quad (4.6)$$

where the matrices \tilde{D} and $\partial \tilde{\mathbf{G}}/\partial \mathbf{C}$ arise from the linearisation of the diffusion matrix and the reaction vector, respectively, and are given by:

$$\begin{aligned} (\tilde{D}(\mathbf{C}))_{ij} &= D_{ij}(\mathbf{C}) + \sum_{k=1}^{N_{\mathbf{S}_h}} \left(\int_{\Omega} \frac{\partial}{\partial \mathbf{c}} \mathbf{D}(\mathbf{C}) \boldsymbol{\varphi}_j \nabla \boldsymbol{\varphi}_k : \nabla \boldsymbol{\varphi}_i \right) \mathbf{C}_k, \\ \left(\frac{\partial \tilde{\mathbf{G}}}{\partial \mathbf{C}}(\mathbf{C}) \right)_{ij} &= \int_{\Omega} \boldsymbol{\varphi}_j^T \nabla \mathbf{G}(\mathbf{C}) \boldsymbol{\varphi}_i \end{aligned} \quad (4.7)$$

and the matrix $\frac{\partial}{\partial \mathbf{c}} \mathbf{D}(\mathbf{C}) \boldsymbol{\varphi}_j$ is a shorthand notation for $\sum_{s=1}^m \frac{\partial \mathbf{D}}{\partial c_s}(\mathbf{C}) \boldsymbol{\varphi}_j^s$. The Newton–Raphson system (4.5) for the full monolithic ADR can be reformulated as a variational problem for the finite element correction vector $\delta\mathbf{c}_h$, leading to the following solver for the ADR system:

(ADR1): Given a velocity \mathbf{u}_h^{n+1} , a solution \mathbf{c}_h^n of the ADR at time t^n , and the approximate solution $\mathbf{c}_h^{n+1,k}$ at the k -th iteration of the Newton–Raphson method for the full monolithic ADR system, find $\delta\mathbf{c}_h \in \mathbf{S}_{h,0}$ such that:

$$\left(\frac{1}{\Delta t} \mathcal{A}_{\mathbf{c}} + C(\mathbf{u}_h^{n+1}) + d\mathcal{D}_{\mathbf{c}_h^{n+1,k}} - d\mathcal{G}_{\mathbf{c}_h^{n+1,k}} \right) \delta\mathbf{c}_h = -\mathcal{R}^n(\mathbf{c}_h^{n+1,k}), \quad (4.8)$$

and update $\mathbf{c}_h^{n+1,k+1} = \mathbf{c}_h^{n+1,k} + \delta\mathbf{c}_h$, until $\|\delta\mathbf{c}_h\|_{\mathbf{L}^2(\Omega)} \leq \text{tol}$.

The linear and bilinear operators in the variational problem (4.8) are given by:

$$\begin{aligned} [\mathcal{R}^n(\mathbf{c}), \mathbf{s}] &:= \frac{1}{\Delta t} [\mathcal{A}_{\mathbf{c}}(\mathbf{c} - \mathbf{c}^n), \mathbf{s}] + [C(\mathbf{c}); \mathbf{u}_h^{n+1}, \mathbf{s}] + [\mathcal{D}(\mathbf{c}), \mathbf{s}] - [\mathcal{G}(\mathbf{c}), \mathbf{s}], \\ [d\mathcal{D}_{\mathbf{c}}(\delta\mathbf{c}), \mathbf{s}] &:= \int_{\Omega} \mathbf{D}(\mathbf{c}) \nabla \delta\mathbf{c} : \nabla \mathbf{s} + \int_{\Omega} \frac{\partial}{\partial \mathbf{c}} \mathbf{D}(\mathbf{c}) \delta\mathbf{c} \nabla \mathbf{c} : \nabla \mathbf{s}, \\ [d\mathcal{G}_{\mathbf{c}}(\delta\mathbf{c}), \mathbf{s}] &:= \int_{\Omega} \mathbf{s}^T \nabla \mathbf{G}(\mathbf{c}) \delta\mathbf{c}. \end{aligned} \quad (4.9)$$

We stress that in problem (4.8) we require that the unknown $\delta\mathbf{c}_h = \mathbf{c}_h^{n+1,k+1} - \mathbf{c}_h^{n+1,k}$ is in $\mathbf{S}_{h,0}$, because it must be zero at the boundaries where the Dirichlet conditions apply. To obtain an adequate initial guess $\mathbf{c}_h^{n+1,0}$ we can solve, at the beginning of the Newton–Raphson scheme, a simplified linear problem, typically with $\mathbf{D}(\mathbf{c}_h^n)$ and $\mathbf{G}(\mathbf{c}_h^n)$.

The (ADR1) solver for the full ADR system using Newton–Raphson method is combined with a flow solver (B1) or (B2), leading to a global solution scheme for the problem, denoted as (B1/B2-ADR1). The steps of the solution strategy of our problem using the (B1/B2-ADR1) are summarised in [Algorithm 1](#).

4.2. Inner splitting of the ADR system

When the diffusion matrix \mathbf{D} is constant and the reaction term $\mathbf{G}(\mathbf{c})$ leads to highly stiff systems, it is convenient to split the ADR dynamics into a pure advection–diffusion phase and into a pure reaction phase. This implies we solve problem (3.2) separating the nonlinear term due to reaction $\mathbf{G}(\mathbf{c})$, which defines a nonlinear system of ODEs, from the (typically more regular and smooth) advection–diffusion process. This method is denoted (ADR2) and consists in solving the ADR system in two steps

```

Data:  $\sigma, \mu, \rho, \alpha, D, G, \Delta t, N, tol;$ 
Initialise:  $u_h^0, \omega_h^0, p_h^0, c_h^0;$ 
for  $n = 1, \dots, N$  time steps do
  Given  $c_h^n$ , solve the Brinkman system (B1):
    
$$\begin{pmatrix} A_u & B_1 & B_2 \\ B_1^* & -A_\omega & \mathbf{0} \\ -B_2^* & \mathbf{0} & \mathbf{0} \end{pmatrix} \begin{pmatrix} u_h^{n+1} \\ \omega_h^{n+1} \\ p_h^{n+1} \end{pmatrix} = \begin{pmatrix} \mathcal{F}_1(c_h^n) \\ \mathbf{0} \\ \mathbf{0} \end{pmatrix};$$

  or its split counterpart (B2):
    •  $\widehat{A}_\omega \omega_h^{n+1} = \mathcal{F}_2(c_h^n),$ 
    •  $\widehat{A}_p p_h^{n+1} = \mathcal{F}_3(c_h^n),$ 
    •  $u_h^{n+1} \leftarrow A_u^{-1} \mathcal{F}_1(c_h^n)$ , and project discrete velocity if using lowest order elements;

  Update:  $u_h^{n+1} \leftarrow u_h^n; \omega_h^{n+1} \leftarrow \omega_h^n; p_h^{n+1} \leftarrow p_h^n;$ 
  Given  $u_h^{n+1}$ , solve the full ADR system via Newton–Raphson (ADR1):
  Initialize:  $c_h^{n+1,0};$ 
  while  $\|\delta c\|_{L^2(\Omega)} \geq tol$  do
    Solve the linearised ADR equations monolithically:
    
$$\left( \frac{1}{\Delta t} A_c + C(u_h^{n+1}) + dD_{c_h^{n+1,k}} - dG_{c_h^{n+1,k}} \right) \delta c_h = -\mathcal{R}^n(c_h^{n+1,k}),$$

    Update:  $c_h^{n+1,k+1} \leftarrow c_h^{n+1,k} + \delta c_h;$ 
  end
  Update:  $c_h^{n+1} \leftarrow c_h^n;$ 
end

```

Algorithm 1: Staggered procedure (B1/B2-ADR1) for the Brinkman problem solved with either (B1) or (B2) and the full ADR problem solved with (ADR1).

(ADR2): – Pure advection-diffusion phase: Given u_h^{n+1} and c_h^n , find $c_h^{n+1,*}$ in S_h solution of the linear problem:

$$\int_{\Omega} \frac{c_h^{n+1,*} - c_h^n}{\Delta t} \cdot s_h + \int_{\Omega} (u_h^{n+1} \cdot \nabla) c_h^{n+1,*} \cdot s_h + \int_{\Omega} D \nabla c_h^{n+1,*} : \nabla s_h = 0, \quad \forall s_h \in S_{0,h}. \quad (4.10)$$

– Pure reaction phase: Setting $c_h^n = c_h^{n+1,*}$, solve the nonlinear problem:

$$\int_{\Omega} \frac{c_h^{n+1} - c_h^n}{\Delta t} \cdot s_h = \int_{\Omega} G(c_h^{n+1}) \cdot s_h, \quad \forall s_h \in S_{0,h}. \quad (4.11)$$

Problems (4.10) and (4.11) are discretised using the same notations (4.4) and (4.3) for matrices and vectors as in the previous section. The nonlinear algebraic system equivalent to the pure reaction phase (4.11), that must be solved at each time iteration t^{n+1} is given by:

$$\frac{A_c}{\Delta t} \mathbf{C}^{n+1} = \frac{A_c}{\Delta t} \mathbf{C}^n + \widetilde{\mathbf{G}}(\mathbf{C}^{n+1}), \quad (4.12)$$

where matrices and vectors A_c , \mathbf{C}^n and $\widetilde{\mathbf{G}}$ are defined in (4.4), (4.3). System (4.12) can be solved iteratively using the Newton–Raphson method. With this aim we define the residual $\mathbf{R}^{*,n}$ of the pure reaction phase as

$$\mathbf{R}^{*,n} := \frac{A_c}{\Delta t} \mathbf{C}^{n+1} - \frac{A_c}{\Delta t} \mathbf{C}^n - \widetilde{\mathbf{G}}(\mathbf{C}^{n+1}),$$

and again we notice that solving (4.12) is equivalent to solve $\mathbf{R}^{*,n}(\mathbf{C}^{n+1}) = \mathbf{0}$. Given an approximate solution of the system (4.12) $\mathbf{C}^{n+1,k}$ at iteration k , one solves the Newton–Raphson system for the pure reaction problem:

$$\left(\frac{A_c}{\Delta t} - \frac{\partial \widetilde{\mathbf{G}}}{\partial \mathbf{C}}(\mathbf{C}^{n+1,k}) \right) \delta \mathbf{C} = -\mathbf{R}^{*,n}(\mathbf{C}^{n+1,k}), \quad (4.13)$$

$$\mathbf{C}^{n+1,k+1} = \mathbf{C}^{n+1,k} + \delta \mathbf{C}.$$

Data: $\sigma, \mu, \rho, \alpha, \mathbf{D}, \mathbf{G}, \Delta t, N, \text{tol}$;
Initialise: $\mathbf{u}_h^0, \boldsymbol{\omega}_h^0, p_h^0, \mathbf{c}_h^0$;
for $n = 1, \dots, N$ time steps **do**
 Given \mathbf{c}_h^n , solve the Brinkman system (B1):

$$\begin{pmatrix} \mathcal{A}_{\mathbf{u}} & \mathcal{B}_1 & \mathcal{B}_2 \\ \mathcal{B}_1^* & -\mathcal{A}_{\boldsymbol{\omega}} & \mathbf{0} \\ -\mathcal{B}_2^* & \mathbf{0} & \mathbf{0} \end{pmatrix} \begin{pmatrix} \mathbf{u}_h^{n+1} \\ \boldsymbol{\omega}_h^{n+1} \\ p_h^{n+1} \end{pmatrix} = \begin{pmatrix} \mathcal{F}_1(\mathbf{c}_h^n) \\ \mathbf{0} \\ \mathbf{0} \end{pmatrix};$$

 or its split counterpart (B2):
 • $\widehat{\mathcal{A}}_{\boldsymbol{\omega}} \boldsymbol{\omega}_h^{n+1} = \mathcal{F}_2(\mathbf{c}_h^n)$,
 • $\widehat{\mathcal{A}}_p p_h^{n+1} = \mathcal{F}_3(\mathbf{c}_h^n)$,
 • $\mathbf{u}_h^{n+1} \leftarrow \mathcal{A}_{\mathbf{u}}^{-1} \mathcal{F}_1(\mathbf{c}_h^n)$, and project discrete velocity if using lowest order elements;
Update: $\mathbf{u}_h^{n+1} \leftarrow \mathbf{u}_h^n; \boldsymbol{\omega}_h^{n+1} \leftarrow \boldsymbol{\omega}_h^n; p_h^{n+1} \leftarrow p_h^n$;
Given \mathbf{u}_h^{n+1} , solve the advection-diffusion phase:

$$(\mathcal{A}_c + \mathcal{C}(\mathbf{u}_h^{n+1}) + \mathcal{D}) \mathbf{c}_h^{n+1,*} = \mathbf{0};$$

Initialize: $\mathbf{c}_h^{n+1,0} = \mathbf{c}_h^{n+1,*}$;
Solve the pure reaction phase via Newton-Raphson:
while $\|\delta \mathbf{c}_h\|_{L^2(\Omega)} \geq \text{tol}$ **do**
 Solve the linearised reaction problem:

$$\left(\frac{\mathcal{A}_c}{\Delta t} - d\mathcal{G}_{\mathbf{c}_h^{n+1,k}} \right) \delta \mathbf{c}_h - \mathcal{R}^{*,n}(\mathbf{c}_h^{n+1,k});$$

 Update: $\mathbf{c}_h^{n+1,k+1} \leftarrow \mathbf{c}_h^{n+1,k+1} + \delta \mathbf{c}_h$;
 end
 Update:
 $\mathbf{c}_h^{n+1} \leftarrow \mathbf{c}_h^n$;
end

Algorithm 2: Staggered procedure (B1/B2-ADR2) for the Brinkman problem solved with either (B1) or (B2) and the full ADR problem solved with (ADR2).

System (4.13) can be rewritten as a variational problem for the finite element correction $\delta \mathbf{c}_h$. Given \mathbf{c}_h^n and the approximate solution $\mathbf{c}_h^{n+1,k}$ at k -th iteration, the problem is to find $\delta \mathbf{c}_h \in \mathbf{S}_{0,h}$ such that:

$$\left(\frac{\mathcal{A}_c}{\Delta t} - d\mathcal{G}_{\mathbf{c}_h^{n+1,k}} \right) \delta \mathbf{c}_h = -\mathcal{R}^{*,n}(\mathbf{c}_h^{n+1,k}).$$

The operator $d\mathcal{G}_c$ is given in (4.9), while the linear operator corresponding to the pure-reaction residual vector is:

$$[\mathcal{R}^{n,*}(\mathbf{c}), \mathbf{s}] := \frac{1}{\Delta t} [\mathcal{A}_c(\mathbf{c} - \mathbf{c}^n), \mathbf{s}] - [\mathcal{G}(\mathbf{c}), \mathbf{s}].$$

Notice that if the reaction vector \mathbf{G} is zero and the diffusion matrix is constant, then the (ADR2) solver reduces to a pure linear advection-diffusion problem (4.10). A global solver for the Brinkman-ADR problem is then obtained combining one of the two Brinkman solvers (B1) or (B2) and (ADR2). These solution strategies are collected in Algorithm 2.

5. Numerical tests

This section contains a collection of numerical examples serving as validation of the coupling strategies discussed in Section 3, and illustrating the behaviour of the model in two applications of wide interest. Before addressing the applicative tests, we perform a convergence analysis indicating the spatial and temporal accuracy of the methods. Let us consider the square domain $\Omega = (-1, 1)^2$, where (2.1) admits the following exact solutions

$$\mathbf{c} = \begin{pmatrix} \cos(\pi x) \cos(\pi y) \sin(2t) \\ \sin(\pi x) \sin(\pi y) \cos(2t) \end{pmatrix}, \quad \mathbf{u} = \begin{pmatrix} -\cos(\pi x) \sin(\pi y) \sin(2t) \\ \sin(\pi x) \cos(\pi y) \sin(2t) \end{pmatrix}, \quad p = -\frac{1}{4} (\cos(2\pi x) + \cos(2\pi y)) \sin^2(2t),$$

and $\boldsymbol{\omega} = \sqrt{\mu} \operatorname{curl} \mathbf{u}$. For sake of this first convergence test, we assume $\mu = \rho = 1$, σ is the identity matrix, we impose $\mathbf{F} = \mathbf{c} + \mathbf{f}$, $\mathbf{G} = \mathbf{c} + \mathbf{g}$, whereas boundary and initial conditions are now non-homogeneous, and the data in (2.2) are set according to the exact solutions above. Also the source and forcing terms \mathbf{g}, \mathbf{f} are computed using these exact solutions

Table 1

Accuracy test. Errors with respect to manufactured exact solutions, convergence rates, and iteration count until convergence (with a residual tolerance of 1e-6), for two different strategies solving the ADR-Brinkman coupled problem, either with [Algorithm 1](#) (B1-ADR1) solver based on [\(2.4\)](#) (where Iter denotes the number of Newton steps to converge in the monolithic ADR solver), or [Algorithm 2](#) (B2-ADR2) based on formulation from [\(2.5\)](#) (where Iter stands for the required reaction step sub-iterations). The iteration count in the bottom table refers to average number of steps.

Space accuracy									
Dof	$e(\mathbf{c})$	rate	$e(\mathbf{u})$	rate	$e(\boldsymbol{\omega})$	rate	$e(p)$	rate	Iter
Algorithm 1 (B1-ADR1)									
51	1.3240	–	5.6127	–	22.3124	–	1.5630	–	5
163	0.9662	0.4542	4.0102	0.4849	17.2105	0.3742	0.9481	0.7215	6
579	0.5177	0.9002	2.1811	0.8786	9.5741	0.8439	0.4777	0.9894	5
2179	0.2553	1.0197	1.1136	0.9695	4.9105	0.9591	0.2537	0.9772	6
8451	0.1274	0.9834	0.5599	0.9924	2.4655	0.9702	0.1304	0.9828	6
33283	0.0617	0.9845	0.2804	0.9981	1.2361	0.9891	0.0664	0.9574	6
132099	0.0315	0.9776	0.1404	0.9976	0.6117	0.9953	0.0341	0.9599	6
526339	0.0157	1.0002	0.0716	0.9701	0.3058	0.9987	0.0180	0.9617	7
Algorithm 2 (B2-ADR2)									
36	16.8527	–	5.6124	–	22.3284	–	2.3027	–	8
100	14.1156	0.2556	4.0105	0.4848	17.2265	0.3742	1.1871	0.9558	5
324	7.3737	0.9368	2.1812	0.8786	9.5974	0.8439	1.1215	0.0819	5
1156	3.7222	0.9862	1.1139	0.9694	4.9365	0.9591	0.5807	0.9496	6
4356	1.8655	0.9965	0.5602	0.9416	2.4860	0.9896	0.2933	0.9853	6
16900	0.9333	0.9991	0.2827	0.9863	1.2452	0.9974	0.1470	0.9958	5
66564	0.4667	0.9997	0.1488	0.9321	0.6229	0.9993	0.0736	0.9987	4
264196	0.2333	0.9999	0.1644	0.9557	0.3114	0.9998	0.0368	0.9991	4
Time accuracy									
Δt	$E(\chi)$	rate	Iter	$E(\chi)$	rate	Iter			
Algorithm 1 (B1-ADR1)									
1	28.4456	–	6.1	32.8502	–	5.8			
0.1	16.3242	0.6877	5.5	20.5543	0.7796	5.6			
0.01	8.2311	0.9425	6.2	10.3370	0.9137	5.6			
0.001	4.2832	0.9203	6.2	5.6941	0.9426	5.8			
0.0001	2.1655	0.9849	6.1	2.3681	0.9832	5.8			
Algorithm 2 (B2-ADR2)									

in combination with [\(2.1\)](#). The experimental mesh convergence analysis is done by successively refining an initial coarse triangular mesh and computing individual errors between the numerical solution produced with the finite element methods defined in Section 3 and the exact solution projected on each refinement level (these errors are denoted by $e(\cdot)$ and are measured in their natural norms, at the final time $T = 1$, and employing a timestep of $\Delta t = 1E-4$). The convergence history displayed in [Table 1](#) confirms the $O(h)$ -accuracy expected by the used spaces characterising each finite element formulation. Likewise, an asymptotic $O(\Delta t)$ convergence rate is obtained for the time discretisation, assessed by fixing a refined mesh of size $h = \sqrt{2}/400$ and considering accumulative errors (in the energy norm $E(\chi) = [\Delta t \sum |\chi_h^n - \chi(t^n)|^2]^{1/2}$) on successively smaller timesteps. The errors themselves are larger for the second partitioned coupling (B2), but the convergence orders remain essentially the same.

5.1. Double-diffusion in porous cavities

We now perform a series of computations focused on a doubly-diffusive model governing the interaction between the concentration of brine (field c_1), temperature (encoded in c_2), and immiscible flow in saturated porous media. A similar study can be found in [\[11,31\]](#). The problem under consideration takes place in a porous square cavity $\Omega = (0, 1)^2$ filled with a Newtonian fluid of velocity, vorticity, and pressure $(\mathbf{u}, \boldsymbol{\omega}, p)$. The left and right walls are maintained at different uniform temperatures and concentrations respectively $c_2^{\text{left}} = c_1^{\text{left}} = 0$ and $c_2^{\text{right}} = c_1^{\text{right}} = 1$. The horizontal walls are assumed adiabatic and insulated (that is, no-flux boundary conditions are set for the ADR system). Slip velocity conditions (i.e., zero normal velocities) and zero vorticity are imposed everywhere on the boundary, and the coupled system adopts the form [\(2.1\)](#) where diffusion, reaction, permeability, and forcing terms are defined as

$$\mathbf{D}(\mathbf{c}) = \text{diag}((\text{Le Pr})^{-1}, R_k \text{Pr}^{-1}), \quad \mathbf{G}(\mathbf{c}) = \mathbf{0}, \quad \sigma = \frac{1}{\text{Da}}, \quad \mathbf{F}(\mathbf{c}) = \text{Gr}(c_2 + \text{N}c_1)\mathbf{g},$$

respectively. The particular structure of the problem implies that the buoyancy term N is a measure of the coupling strength between the flow and the ADR equations. Notice that for a given velocity, the ADR equations are now linear and the associated errors would be more easily tractable to the (B1-ADR2) splitting method at hand.

In order to investigate the robustness of the proposed (B1-ADR2) splitting method with respect to the coupling strength, we fix the parameters $\text{Le} = 10$, $\mu = \Lambda = 1$, $\text{Da} = 1E-3$, $R_k = 1$, $\text{Pr} = 0.71$, $\epsilon = 0.5$, $\text{Ra} = 100$, $\text{Gr} = \text{Ra}/(\text{PrDa})$, we use a timestep $\Delta t = 1E-3$ and a structured grid of meshsize $h = 1/100$, and let the buoyancy term N vary. By χ_h^{MONO} and χ_h^{SPLIT} we will denote the finite element solution (at the final time $T = 0.5$) generated by the fully monolithic approach, and the

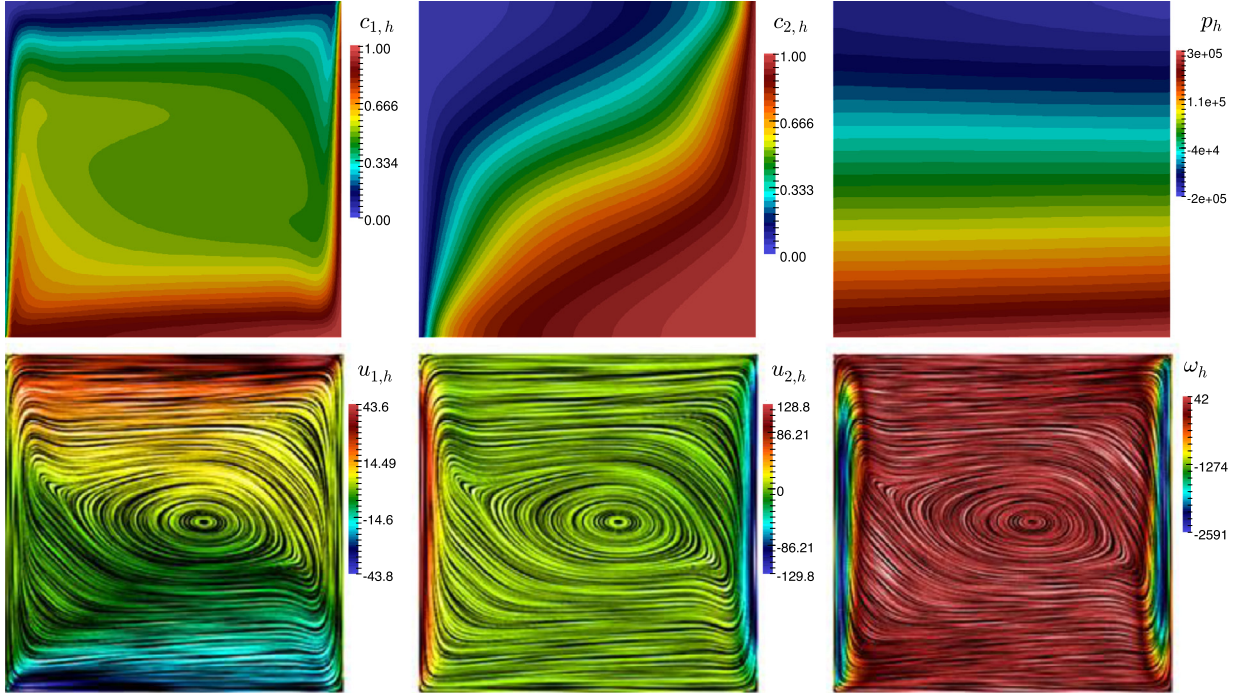


Fig. 5.1. Example 1A. Double diffusion in a porous cavity, 2D case. Approximate solutions at the final time (brine concentration, temperature, pressure, velocity components, and vorticity). (For interpretation of the references to colour in this figure legend, the reader is referred to the web version of this article.)

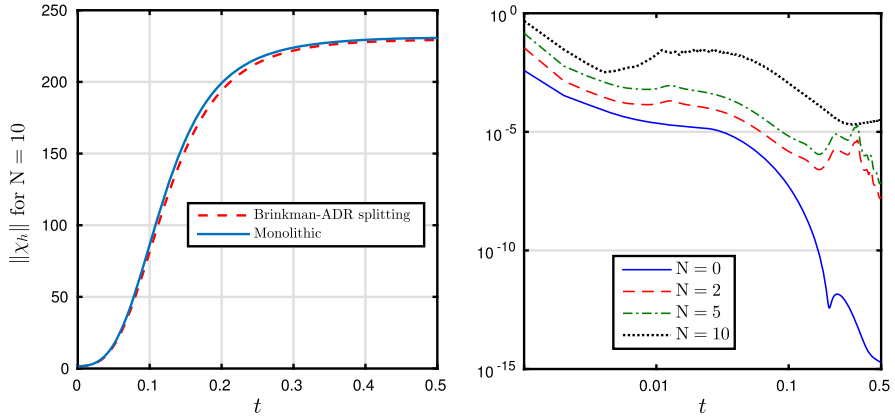


Fig. 5.2. Example 1A. Evolution of the norm of the solution \$\chi_h\$ in the double diffusion problem with high buoyancy \$N = 10\$, using both the monolithic and the splitting method (B1-ADR2) (left panel). On the right we plot the evolution of the error between the monolithic and splitting solutions, \$e(\chi)\$.

operator splitting method (B1-ADR2), respectively. A comparison is then performed in terms of the evolution of global errors defined as the \$L^2\$-norm of the difference between the two solutions \$e(\chi) = \|\chi_h^{\text{MONO}} - \chi_h^{\text{SPLIT}}\|\$, where the approximation produced by the monolithic method is considered as a reference solution. In Fig. 5.2 we report the temporal evolution of \$e(\chi)\$ for different values of the buoyancy \$N \in \{0, 2, 5, 10\}\$. As \$N\$ increases, the error grows, implying that the coupling strength affects substantially the quality of the solution generated by the segregated solver. For reference we also depict each individual field of the numerical solution generated with the splitting method, shown at the final time \$T = 0.5\$, in Fig. 5.1.

The results of the finite element model proposed are compared with published results on the purely thermal problem (decoupled thermal and mass \$N = 0\$). Consider the square domain \$\Omega = (0, 1)^2\$ and set the boundary conditions as:

$$c_1 = c_2 = 1 : x = 0, \quad c_1 = c_2 = 0 : x = 1, \quad \mathbf{u} = \mathbf{0} : \partial\Omega.$$

We fix the parameters \$N = 0\$, \$Le = 10\$, \$\mu = \Lambda = 1\$, \$R_k = 1\$, \$Pr = 0.71\$, \$\epsilon = 0.5\$, \$Ra = 100\$, \$Gr = Ra/(PrDa)\$ and let vary \$Da \in \{10^{-1}, 10^{-3}, 10^{-5}\}\$ and \$Ra \in \{100, 200\}\$. The comparisons are based on the average Nusselt and Sherwood numbers:

Table 1

Example 1A. Average Nusselt and Sherwood numbers $\overline{\text{Nu}}$ and $\overline{\text{Sh}}$ obtained with the (B1-ADR2) splitting in the case of decoupled mass and heat transfer processes ($N = 0$, $\text{Le} = 10$) and comparison against reference results published in Shao et al. [31].

Da	Ra	Reference Nu	Computed Nu	Reference Sh	Computed Sh
10^{-1}	100	1.52	1.52	5.56	5.60
	200	2.07	2.10	7.32	7.50
10^{-3}	100	2.96	3.01	12.33	11.90
	200	4.43	4.64	17.58	16.57
10^{-5}	100	3.11	3.13	13.40	13.25
	200	4.96	5.01	19.52	19.25

Table 2

Example 1A. Norm of the vorticity and velocity of the computed solution and of the errors computed against a monolithic solution, for different values of the viscosity coefficient.

μ	1E - 15	1E - 10	1E - 5	1
$\ \mathbf{u}_h - \mathbf{u}_h^*\ _{\mathbf{H}(\text{div}; \Omega)}$	6.7914E-06	1.3008E-11	4.6569E-12	3.5855E-12
$\ \mathbf{u}_h\ _{\mathbf{H}(\text{div}; \Omega)}$	21.0725	21.0725	21.0725	19.6517
$\ \omega_h - \omega_h^*\ _{1,\mu}$	5.4204E-10	1.1633E-09	3.8491E-10	1.0258E-09
$\ \omega_h\ _{1,\mu}$	219.1310	219.1316	222.8685	2208.28

$$\overline{\text{Nu}} = - \int_0^1 \frac{\partial c_1}{\partial x} |_{x=0} dy, \quad \overline{\text{Sh}} = - \int_0^1 \frac{\partial c_2}{\partial x} |_{x=0} dy. \quad (5.1)$$

The (B1-ADR2) scheme is used on a regular mesh containing 20000 triangles, considering a timestep of $\Delta t = 0.01$ and the system is run until $T = 2$. The computed numbers are collected in [Table 1](#).

In addition, we assess the robustness of the method with respect to the fluid viscosity. This is performed by taking $N = 0$ and considering a range of viscosity values $\mu = \Lambda \in \{1\text{E}-15, 1\text{E}-10, 1\text{E}-5, 1\}$, where the first one corresponds to the Darcy limit. In all cases the computations are stable and the velocity and vorticity norms remain of the same order of magnitude. This can be evidenced from [Table 2](#), where we also show some relevant errors when comparing the approximations against a reference solution (generated with the monolithic method and denoted with the superscript *) at the final time $T = 0.5$.

We also carry out a simulation of double-diffusion-driven natural convection in a porous 3D enclosure. The problem setting follows [\[22\]](#), and we reuse most of the parameters from the 2D computation, except for $\text{Ra} = 1\text{E}+4$ and $N = 1$. The structured tetrahedral mesh discretising the domain $\Omega = (0, 0.75)^3$ consists of 295488 elements and 50653 vertices, and we employ a fixed timestep of $\Delta t = 1\text{E}-3$. A portray of the generated solutions (using [Algorithm 2](#) and the solver (B2-ADR2)) is presented in [Fig. 5.3](#), indicating well-resolved profiles and absence of spurious oscillations.

5.2. Exothermic reaction–diffusion fronts in porous media

Let us now consider a rectangular domain $\Omega = (0, L) \times (0, H)$ and endow [\(2.1\)](#) with the following specification of diffusion, reaction, permeability and forcing terms, respectively:

$$\mathbf{D}(\mathbf{c}) = \text{diag}(1, \text{Le}), \quad \mathbf{G}(\mathbf{c}) = \text{Da} f(c_1)(-1, 1)^T, \quad \sigma = \frac{1}{\text{Da}}, \quad \mathbf{F}(\mathbf{c}) = (\gamma_T - c_1)\mathbf{g}, \quad (5.2)$$

where $f(c_1) = 36c_1(\kappa + 7c_1)(1 - c_1)^2$, $\kappa = 1$ and $\mathbf{g} = (0, -1)^T$. Denoting c_1 and c_2 respectively as concentration of solutal and temperature inside the fluid, the system defined by [\(2.1\)](#) and [\(5.2\)](#) represents the dynamics of a two-dimensional porous medium in the presence of gravity (along the stream-wise direction), in which solutal and thermal densities have a competing behaviour. Let us consider initial concentrations of solutal and high temperature near the top of the rectangular domain

$$c_i^0(x, y) = \begin{cases} 0.999 + \zeta_i(0.001) & \text{if } H - \epsilon \leq y \leq H, \\ 0 & \text{otherwise} \end{cases}, \quad i = 1, 2,$$

where ζ_1, ζ_2 are random variables uniformly distributed in the interval $[0, 1]$. The resulting chemical front moves downwards invading the fresh reactants. Instabilities result from the competition between solutal and thermal effects through the kinetic term $f(c_1)$ and the buoyancy term $(\gamma_T - c_1)\mathbf{g}$. Downward travelling fronts are buoyantly unstable and develop solutal density fingers in time, as evidenced in [Fig. 5.4](#). Model and numerical parameters are given as $H = 1000$, $L = 2000$, $\Delta t = 40$, $T = 8000$, $\text{Le} = 8$, $\text{Da} = 0.001$, $\gamma_T = 5$.

Because the diffusion matrix is constant and the reaction term is highly nonlinear, we numerically solve this problem using the sub-splitting for the ADR problem described in Section [4.2](#) leading to the global (B1-ADR2) solver.

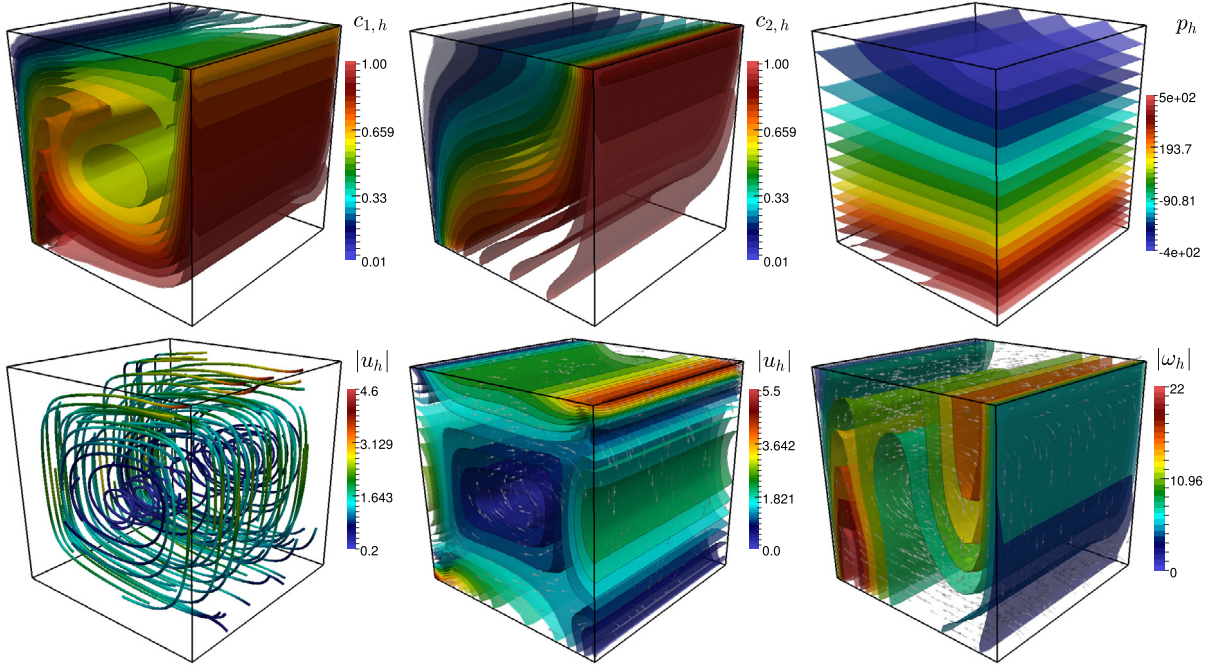


Fig. 5.3. Example 1B. Double diffusion in a porous enclosure, 3D case. Approximate solutions at the final time (brine concentration, temperature, pressure, velocity streamlines, velocity magnitude, and vorticity magnitude). (For interpretation of the references to colour in this figure legend, the reader is referred to the web version of this article.)

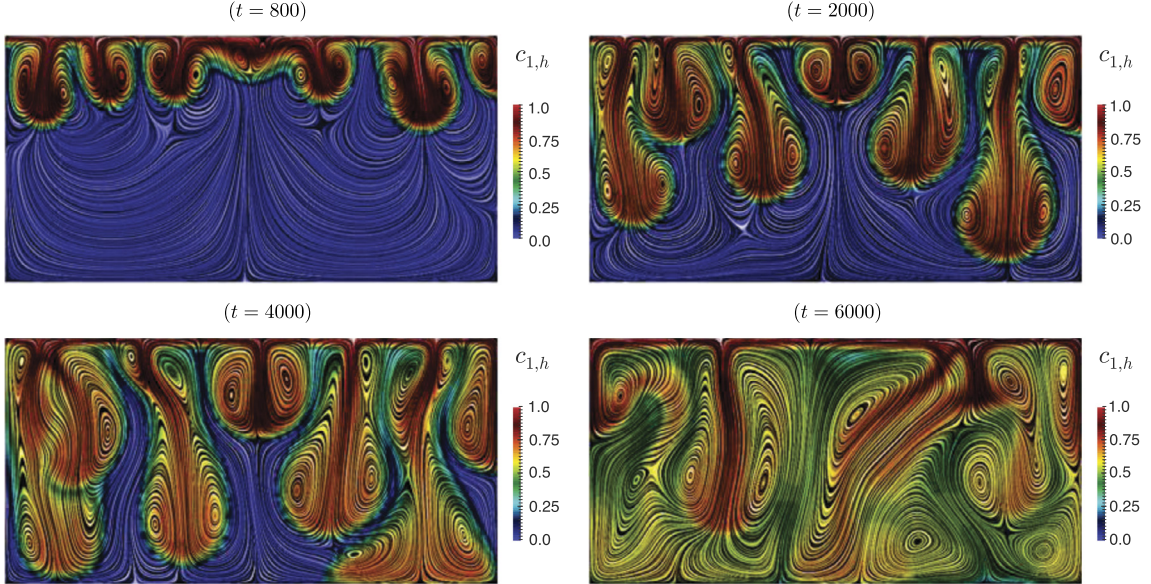


Fig. 5.4. Example 2A. Exothermic fingers within porous media. Snapshots of concentration c_1 at different times. (For interpretation of the references to colour in this figure legend, the reader is referred to the web version of this article.)

The domain is discretised into 26848 elements with 13675 vertices. The number of degrees of freedom for the Brinkman problem is 81045, while for the ADR equations is 27350. In Fig. 5.5 we report on the CPU times for solving the Brinkman-ADR problem defined by (5.2) using the (B1-ADR2) solver with the inner splitting of the ADR problem into a pure advection-diffusion phase and into a pure reaction phase (ADR2). We notice that the computational cost of the nonlinear, pure reaction phase is much higher than that of the linear advection-diffusion phase. As a matter of fact, the rate of convergence of the Newton-Raphson iterative procedure to solve the former is only linear in the sense that $\|\mathbf{c}_h^{n+1,k+1} - \mathbf{c}_h^{n+1,k}\|_{L^2(\Omega)} \approx 1E-k$ (i.e. to reach k digits of precision in the solution of the pure reaction problem approximately k Newton-Raphson iterations are needed), as shown in Fig. 5.5. The evolution of the norms of the concentration, gradient of the concentration,

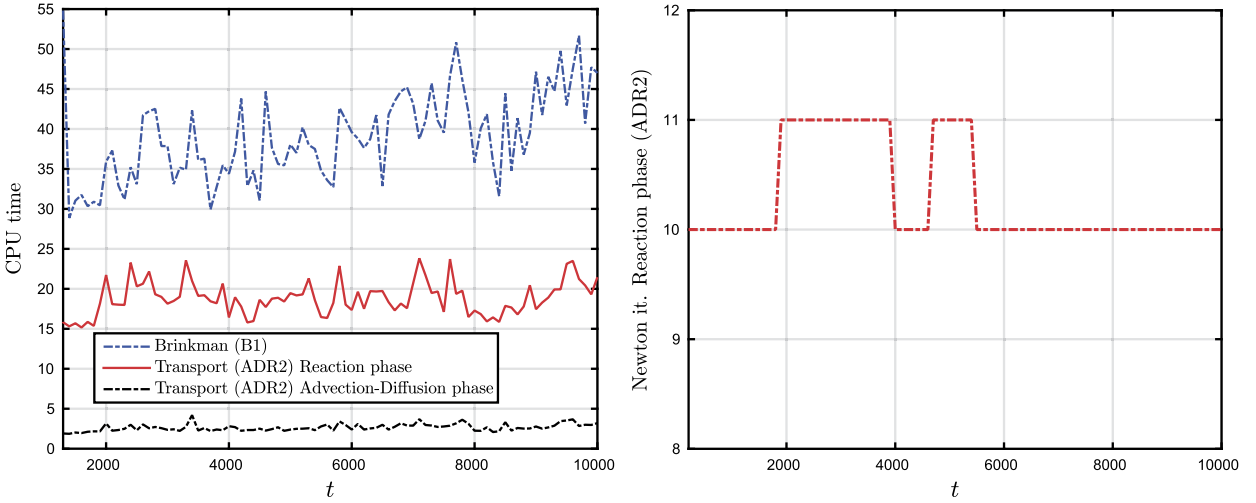


Fig. 5.5. Example 2A. Evolution of the required CPU time for the solution of the Brinkman problem using (B1) and for the ADR problem using the sub-splitting into a pure Advection–Diffusion phase and a pure Reaction phase (ADR2) at each time step. Number of Newton–Raphson iteration needed to reach convergence in the pure Reaction phase with a fixed tolerance $\text{tol} = 1e - 10$. (For interpretation of the references to colour in this figure legend, the reader is referred to the web version of this article.)

and vorticity vector are shown in Fig. 5.6. In correspondence with the developing of finger instabilities, there is a peak in $\|\nabla \mathbf{c}_h\|_{\mathbf{L}^2(\Omega)}$ and a subsequent decay towards a spatially homogeneous configuration.

The effects of modifying the size ratio (typically on the wavenumber of the solutions) are observed in the wide fingers displayed in Fig. 5.7.

5.3. Bioconvection of oxytactic bacteria

For our next round of simulations, let us consider a rectangular box where both bacteria and oxygen coexist within a porous array of fixed particles, filled with an incompressible fluid. After removing the top lid of the box, an interaction between bacteria and the diffusion of oxygen into the liquid onsets the formation of high bacterial concentrations moving towards the bottom of the box. As proposed in [17], an adequate model for this phenomenon is (2.1) with a cross-diffusion term, where we identify the concentration of bacteria with the field c_1 and that of oxygen with c_2 . The diffusion, reaction, and remaining concentration-dependent coefficients are

$$\mathbf{D}(\mathbf{c}) = \begin{pmatrix} D_1 & -\alpha r(c_2)c_1 \\ 0 & D_2 \end{pmatrix}, \quad \mathbf{G}(\mathbf{c}) = \beta r(c_2) \begin{pmatrix} 0 \\ -1 \end{pmatrix}, \quad \sigma = \frac{1}{Sc}, \quad \mathbf{F}(\mathbf{c}) = \gamma c_1 \mathbf{g}.$$

$$\text{where } r(c_2) = \frac{1}{2} \left(1 + \frac{c_2 - c_2^*}{\sqrt{(c_2 - c_2^*)^2 + \varepsilon^2}} \right) \text{ and } \mathbf{g} = (0, -1)^T.$$

It is known (cf. [17]) that for suitable parameters, the solution of the ADR problem c_1, c_2 converges to a steady-state solution (homogeneous in x) of the following system:

$$\Delta c_1 = \alpha \nabla \cdot [c_1 r(c_2) \nabla c_2], \quad \delta \Delta c_2 = \beta r(c_2) c_1,$$

where $\delta = D_2/D_1$. Let us consider the domain $\Omega = [0, 2] \times [0, 1]$, along with the initial conditions

$$c_1^0(x, y) = \begin{cases} 1 & \text{if } y \geq 0.501 - 0.01 \sin((x - 0.5)\pi), \\ 0.5 & \text{otherwise} \end{cases}, \quad c_2^0(x, y) = 1.$$

Fixing the parameters $\beta = 10$, $\delta = 1$, $\gamma = 418$ and $Sc = 7700$, and varying α leads to such a quasi-stationary solution. The splitting (B1-ADR1) with fully implicit treatment of the ADR system, described in Algorithm 1, is run until convergence to a steady-state solution, using $\Delta t = 1E-3$. The vertical profiles of the cell c_1 density and oxygen c_2 at $t = 0.22$ for $\alpha = \{1, 2, 5.952\}$ are shown in Fig. 5.8.

The increase in the value of α (with β and δ fixed) indicates that the directed cell swimming increases relative to the diffusive swimming. Thus, as α increases, the cell density near the surface increases, the cells vacate the lower regions of the chamber more rapidly, and less overall oxygen consumption occurs in these regions. These results are in qualitative agreement with [23, Figure 7].

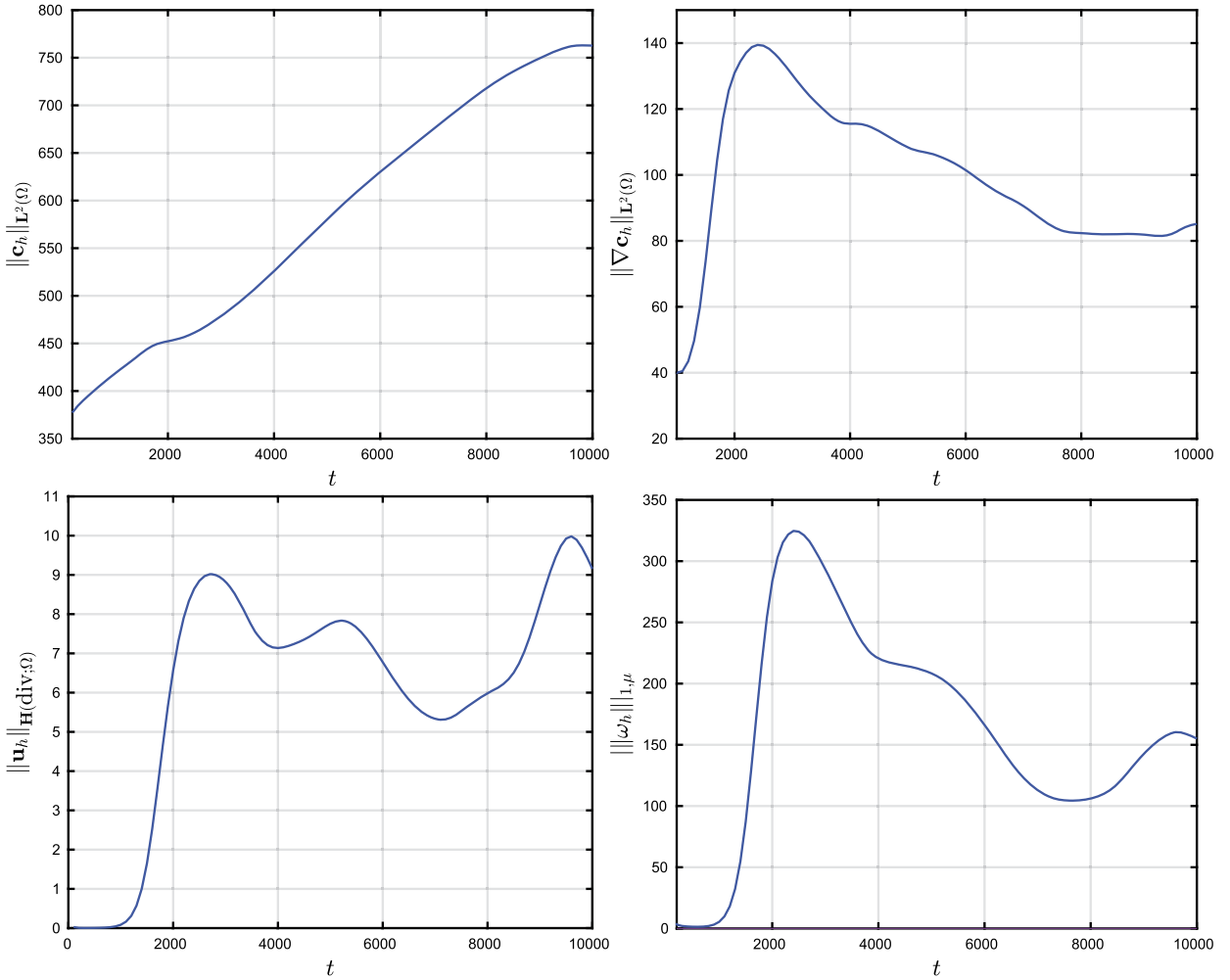


Fig. 5.6. Example 2A. Evolution of the norms of concentration vector $\|c_h\|_{L^2(\Omega)}$, of the gradient $\|\nabla c_h\|_{L^2(\Omega)}$ of the velocity vector $\|u_h\|_{H(\text{div}; \Omega)}$ and the vorticity $\|\omega\|_{1,\mu}$.

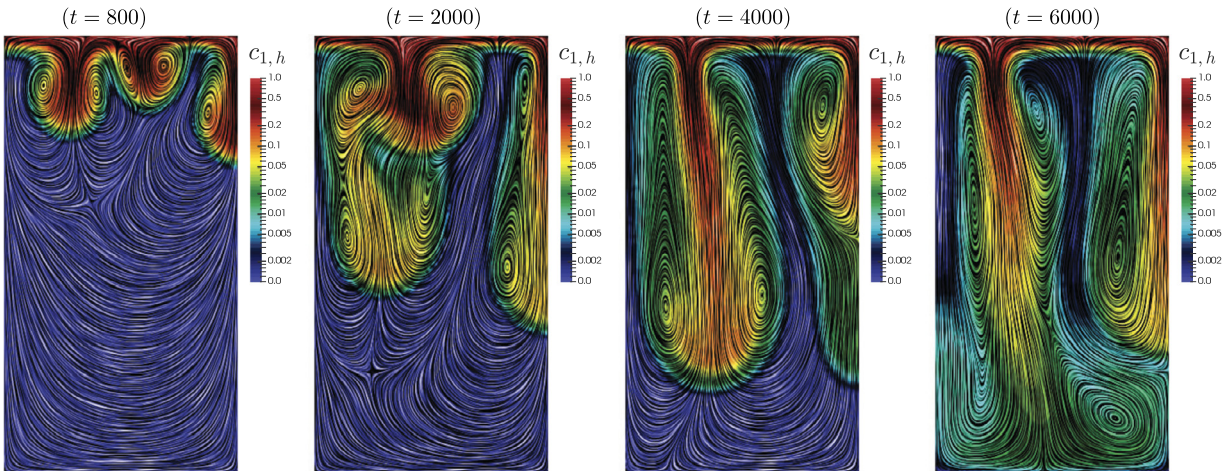


Fig. 5.7. Example 2B. Exothermic fingers within porous media. Snapshots of concentration c_1 and velocity streamlines computed at different time steps. (For interpretation of the references to colour in this figure legend, the reader is referred to the web version of this article.)

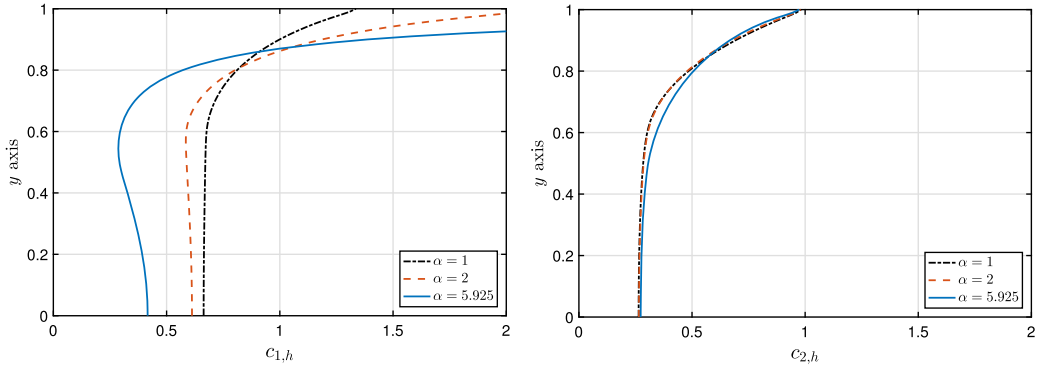


Fig. 5.8. Example 3A. Vertical profiles of (left) cell density $c_{1,h}$ and (right) oxygen $c_{2,h}$ at $t = 0.22$ for $\beta = 10$, $\delta = 1$, $\gamma = 418$, $Sc = 7700$, and $\alpha = 1, 2, 5.952$. (For interpretation of the references to colour in this figure legend, the reader is referred to the web version of this article.)

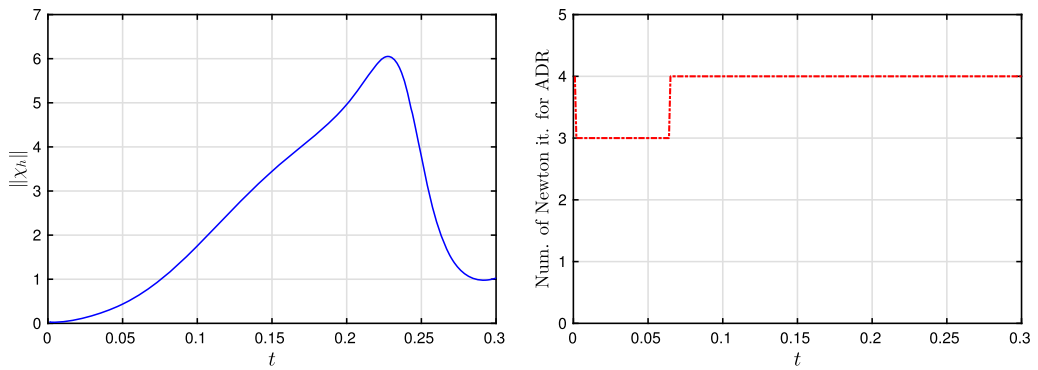


Fig. 5.9. Example 3A. Plot of the (rescaled) norm of the solution χ_h over time (left) and number of Newton-Raphson iterations in the solution of the monolithic scheme (ADR1) (right).

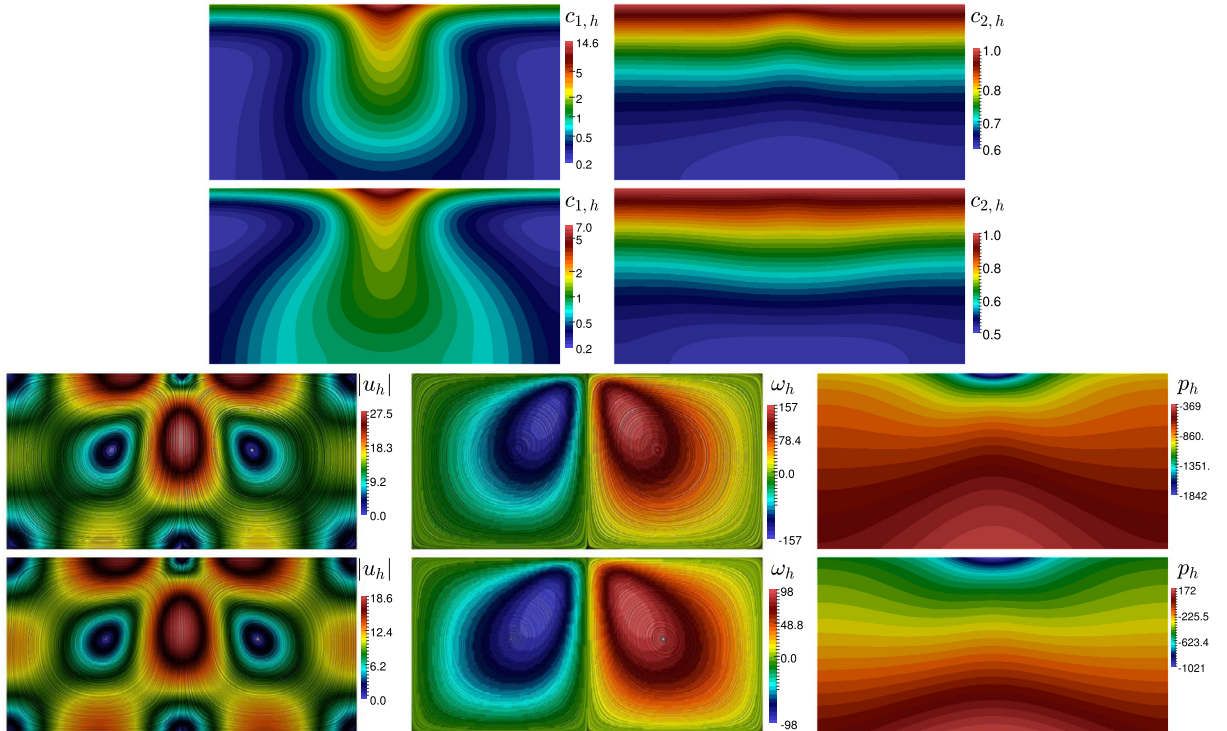


Fig. 5.10. Example 3A. Snapshots at mid (top) and advanced (bottom) times of cell density, oxygen concentration, velocity magnitude, vorticity, and pressure. (For interpretation of the references to colour in this figure legend, the reader is referred to the web version of this article.)

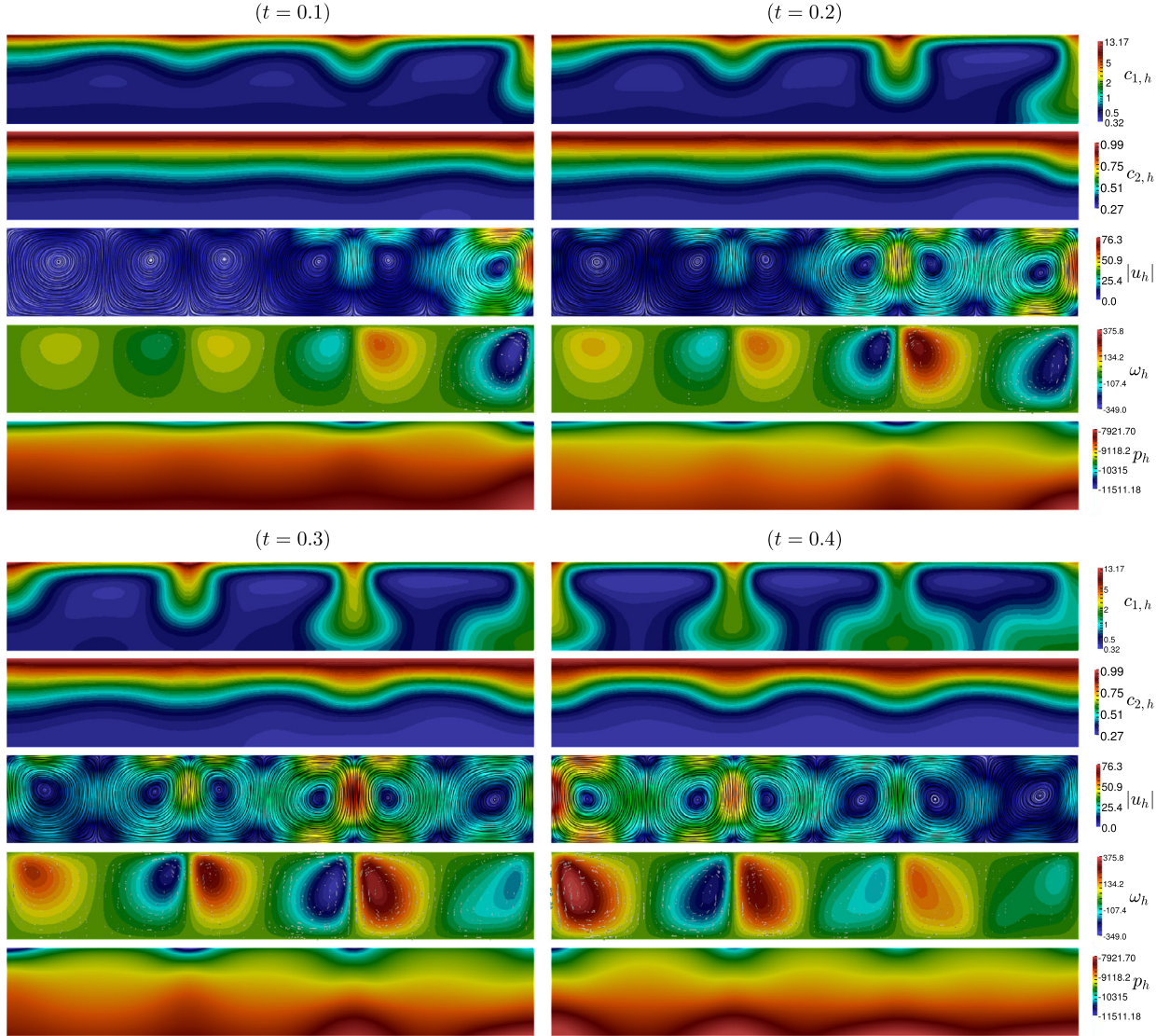


Fig. 5.11. Example 3A. Patterns generated by the bacterial chemotaxis towards oxygen concentration on a domain with modified aspect ratio. Four snapshots of the obtained solutions at different times are presented. (For interpretation of the references to colour in this figure legend, the reader is referred to the web version of this article.)

If we assign the model parameters $\alpha = 10$, $\beta = 10$, $\gamma = 1000$, $\delta = 5$ and $\text{Sc} = 500$, the solution of the ADR equations shows bioconvection patterns evolving in time. At around $t = 0.2$ the solution starts developing instabilities, at $t = 0.25$ a drop of bacterial concentration c_1 starts falling down and hits the bottom of the chamber at $t = 0.3$. In Fig. 5.9 (left) we report the scaled norm of the solution $\|\chi_h\|^2$. It is evident that $\|\chi_h\|^2$ has a peak, which is in correspondence to the development of solution instabilities due to spatial inhomogeneity. In Fig. 5.9 (right) we show the number of Newton–Raphson iterations to reach a solution of the ADR monolithic system using the (ADR1) solver, within a tolerance of $\text{tol} = 1\text{E-}13$. We can observe an increase of the number of iterations at the onset of instabilities generated by the strongly nonlinear behaviour of the system.

Snapshots of the numerical solutions obtained with the splitting method (B1-ADR1) are displayed in Fig. 5.10. Even if the oxygen distribution does not show a very marked gradient in the x -direction, the vorticity plots (bottom centre panels) indicate a high flow recirculation at the centre of the domain. We also stress that modifying the aspect ratio of the box influences the onset of fingering phenomena in the system, as clearly seen from Fig. 5.11.

Another set of simulations (referred to as Example 3B), is performed, now on a 3D setting. We consider a cylindrical geometry of radius 0.5 and height 0.75, discretised into a tetrahedral mesh of 169392 cells and 29109 points. The configuration of the governing equations and specification of constant and variable coefficients is given as follows: $\alpha = 0.25$, $\beta = 1.5$, $\gamma = 1500$, $D_1 = 0.005$, $D_2 = 0.4$, $S = 7700$, $\sigma = S^{-1} \times 1\text{E+}6$, $s^* = 0.3$, $\mu = 2$. A fixed timestep of $\Delta t = 5\text{E-}4$ is

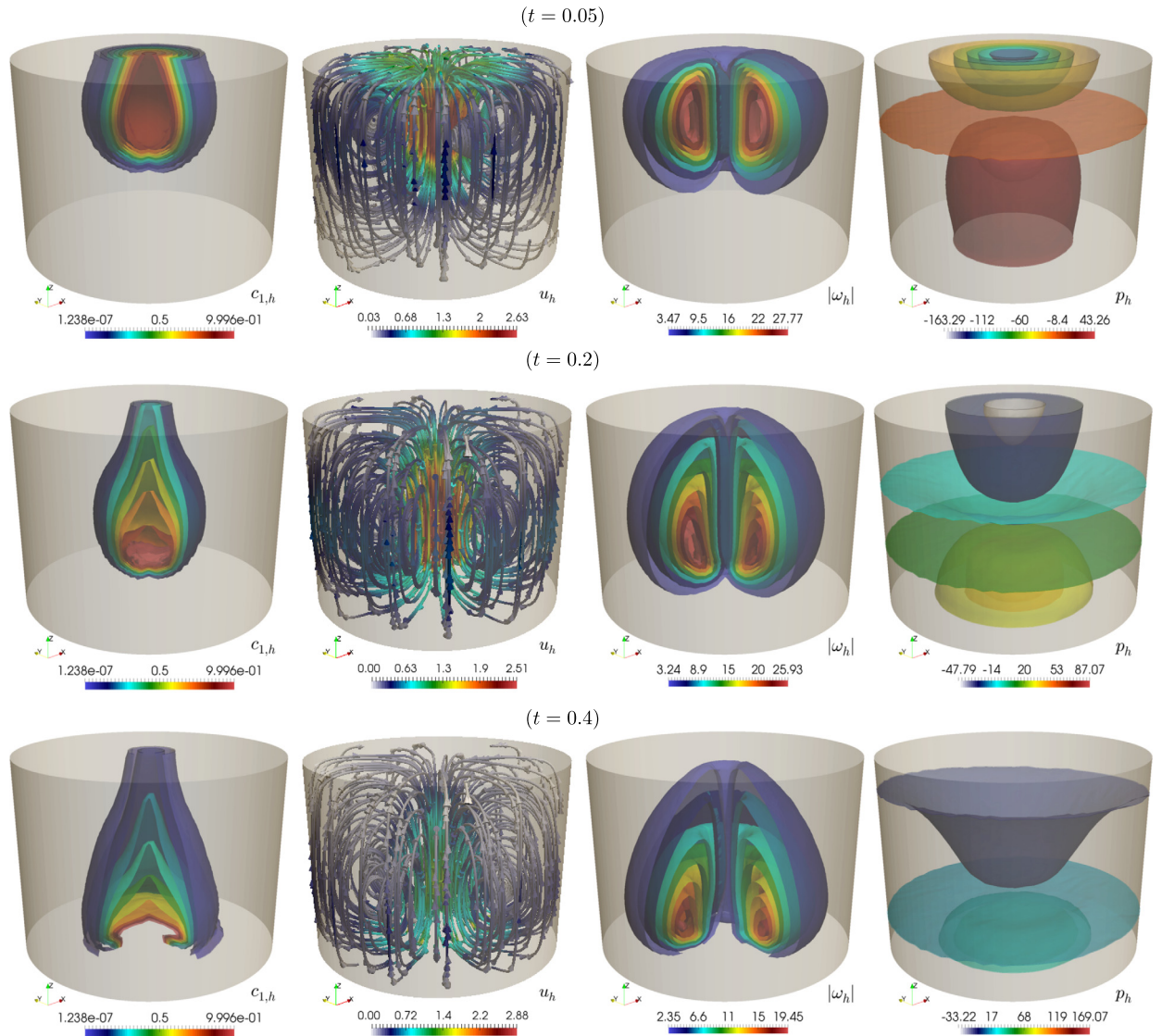


Fig. 5.12. Example 3B. Snapshots at three instances of cell density (left), velocity patterns and vorticity magnitude (middle columns), and pressure distribution (right panels). (For interpretation of the references to colour in this figure legend, the reader is referred to the web version of this article.)

used, and we assess the capabilities of two different coupling methods based on the split Brinkman solvers defined by (2.4) (B1) and (2.5) (B2), respectively. For the first coupling (B1), the solve involves the preliminary assembly of the Brinkman system (arising from a finite element discretisation using lowest order Raviart–Thomas approximation of velocity, first degree Nédélec elements for vorticity, and piecewise constants for pressure) representing 678020 degrees of freedom, and the assembly of the ADR equations, where the piecewise linear approximation of bacteria and oxygen concentrations leads to a system of 58218 unknowns. The second coupling strategy (B2) has a Brinkman solve split into a vorticity matrix of size 193724 (also using Nédélec finite elements), a pressure solution with 29109 degrees of freedom, and a matrix–vector multiplication to project the reconstructed velocity on the Raviart–Thomas space. As a reference, let us point out that the monolithic solver requires the assembly and solution (at each Newton step) of a system with 736238 degrees of freedom.

We simulate the evolution of the system starting from an initial uniform oxygen concentration $c_2 = 1$ and an initial distribution of bacteria packed in a ball of radius 0.2 and placed near the top of the vessel. Snapshots of the concentration of bacteria and the associated flow patterns, computed with the first staggered solution method (B1-ADR1), are portrayed in Fig. 5.12. We observe that as the bacteria propagate downwards, the velocity and vorticity fields indicate recirculating zones following the high gradients of c_1 , whereas the pressure exhibits smooth transitions from high to low values on the bottom and top of the domain, respectively. As soon as the high bacteria concentration reaches the bottom of the vessel (occurring approximately at $t = 0.2$), the dynamics of the system implies a slightly weaker coupling between flow and transport. This is particularly noticed in the top right plot of Fig. 5.13, where the CPU times for assembly and solution of the Brinkman

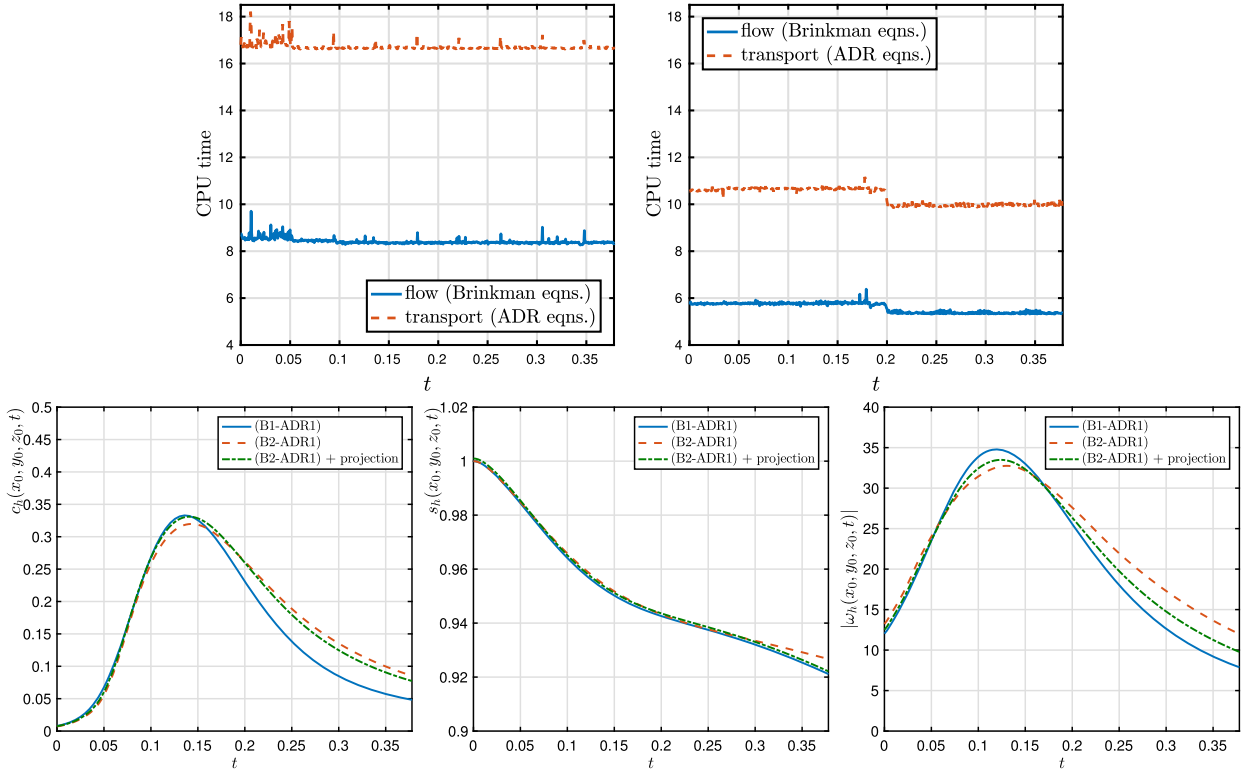


Fig. 5.13. Example 3B. Evolution of the required CPU time (adimensional units) for the solution of the flow and transport problems at each time step (solid and dashed lines, respectively), for the first (B1-ADR1) and second (B2-ADR1) splitting algorithms (top left and top right plots, respectively). The bottom panels show the evolution of the bacteria concentration, oxygen, and vorticity magnitude on a single point near the domain centre, using also splitting (B2) with and without velocity projection.

and ADR systems displays a slight step down happening around $t = 0.2$. The timings reported in the top panels of the figure encompass the RHS assembly and solution for the Brinkman equations, and the assembly of the stiffness matrix and solution of the ADR equations. On top of these values, the initial assembly of the stiffness matrix of the Brinkman problem and the RHS of the ADR equations represents an average of additional 124.91 time units for the first partitioned solver, and 28.31 time units for the second decoupling strategy. In general, the CPU time for the flow solution is roughly half that for the transport. We also observe that for the second coupling (B2) the CPU usage for the total solution is approximately 75% lower than the one in the first coupling. The second row of Fig. 5.13 presents the history of bacteria concentration, oxygen quantity, and vorticity magnitude computed on the point $(x_0, y_0, z_0) = (0.6, 0.6, 0.6)$, indicating that the solution itself differs from one coupling to the other. As the simulation was performed using lowest-order elements, we show the transients obtained with the second Brinkman splitting with and without additional projection of the velocity. In any case, the splitting (B2) produces a slower decay of the bacteria concentration and vorticity fronts, but the velocity projection generates profiles closer to those obtained with splitting (B1).

6. Concluding remarks

In this paper we have presented a set of coupling strategies for the partitioned solution of advection-reaction-diffusion equations interacting within viscous flows in porous media governed by Brinkman equations in their velocity-vorticity-pressure formulation. The flow equations follow a discretisation with, either a family of $\mathbb{RT}_0 - \mathbb{ND}_1 - \mathbb{P}_0$ finite elements (encoded in the (B1) solver), or via a split between two elliptic solvers for vorticity and pressure plus a postprocessing yielding velocity (referred to as the (B2) solver). In turn, the ADR system is solved with a primal finite element method using piecewise linear approximations of the species concentration, and a splitting of reaction and diffusion steps is conducted in different ways, according to the coupling strength exhibited by each particular application. Both accuracy and robustness of the proposed schemes have been demonstrated by means of several numerical tests, involving bioconvection of oxytactic bacteria and doubly-diffusive viscous flows in porous media. A set of comparisons between different coupling strategies has been carried out, and quantified in terms of memory usage, iteration count, speed of calculation, and dynamics of the energy norm in the system. These examples convey that split-based formulations are substantially advantageous for the family of problems at hand. Further extensions of this work include ADR systems where the diffusion depends on the strain rate, and the generalisation of Brinkman equations to linear and nonlinear poroelasticity describing flow within deformable

porous media, and for which a large range of applications is readily envisaged. In terms of numerical approximations, we also foresee the incorporation of conservative schemes for flow and transport in the spirit of the recent contributions [10, 33, 34].

Acknowledgements

This work was advanced during a visit of the first author to the Mathematical Institute of Oxford University, partially supported by the European Research Council through the ERC Starting Grant “Multi-field and multi-scale Computational Approach to Design and Durability of PhotoVoltaic Modules” GA 306622. The authors also acknowledge the support by the Engineering and Physical Sciences Research Council EPSRC, through the research grant EP/R005702/1. Finally, fruitful discussions with V. Anaya and D. Mora (Universidad del Bío-Bío, Chile) on different Brinkman solvers, are gratefully acknowledged.

References

- [1] B. Al-Sulaimi, The non-linear energy stability of Brinkman thermosolutal convection with reaction, *Ric. Mat.* 65 (2) (2016) 381–397.
- [2] H. Alhumade, J. Azaiez, Reversible reactive flow displacements in homogeneous porous media, in: *Proc. WCE, 2013*, pp. 1–6.
- [3] T. Almani, K. Kumar, A. Dogru, G. Singh, M.F. Wheeler, Convergence analysis of multirate fixed-stress split iterative schemes for coupling flow with geomechanics, *Comput. Methods Appl. Mech. Eng.* 311 (2016) 180–207.
- [4] V. Anaya, M. Bendahmane, D. Mora, R. Ruiz-Baier, On a primal-mixed vorticity-based formulation for reaction-diffusion-Brinkman systems, submitted for publication, available from <https://hal.archives-ouvertes.fr/hal-01407343>, 2016.
- [5] V. Anaya, D. Mora, R. Oyarzúa, R. Ruiz-Baier, A priori and a posteriori error analysis of a mixed scheme for the Brinkman problem, *Numer. Math.* 133 (4) (2016) 781–817.
- [6] V. Anaya, D. Mora, C. Reales, R. Ruiz-Baier, Stabilized mixed approximation of axisymmetric Brinkman flows, *ESAIM: Math. Model. Numer. Anal.* 49 (2015) 855–874.
- [7] V. Anaya, D. Mora, R. Ruiz-Baier, Pure vorticity formulation and Galerkin discretization for the Brinkman equations, *IMA J. Numer. Anal.* (2017), <http://dx.doi.org/10.1093/imanum/drw056>, in press.
- [8] C.G. Bell, H.M. Byrne, J.P. Whiteley, S.L. Waters, Heat or mass transfer at low Péclet number for Brinkman and Darcy flow round a sphere, *Int. J. Heat Mass Transf.* 68 (2014) 247–258.
- [9] M. Bukac, W. Layton, M. Moraiti, H. Tran, C. Trenchea, Analysis of partitioned methods for the Biot system, *Numer. Methods Partial Differ. Equ.* 31 (2015) 1769–1813.
- [10] R. Bürger, S. Kumar, S. Kumar Kenettinkara, R. Ruiz-Baier, Discontinuous approximation of viscous two-phase flow in heterogeneous porous media, *J. Comput. Phys.* 321 (2016) 126–150.
- [11] A. Çikici, S. Kaya, Finite element analysis of a projection-based stabilization method for the Darcy-Brinkman equations in double-diffusive convection, *Appl. Numer. Math.* 64 (2013) 35–49.
- [12] J.R. Douglas, R. Ewing, M.F. Wheeler, The approximation of the pressure by a mixed method in the simulation of miscible displacement, *RAIRO. Anal. Numér.* 17 (1983) 17–33.
- [13] D.R. Duran, *Numerical Methods for Fluid Dynamics*, Texts in Applied Mathematics, vol. 32, Springer, Cham, Heidelberg, New York, Dordrecht, London, 2010.
- [14] P. Erbts, S. Hartmann, A. Düster, A partitioned solution approach for electro-thermo-mechanical problems, *Arch. Appl. Mech.* 85 (2015) 1075–1101.
- [15] R. Ewing, M.F. Wheeler, Galerkin methods for miscible displacement problems in porous media, *SIAM J. Numer. Anal.* 17 (1980) 351–365.
- [16] V. Girault, P.A. Raviart, *Finite Element Methods for Navier-Stokes Equations. Theory and Algorithms*, Springer, Berlin, 1986.
- [17] A.J. Hillesdon, T.D. Pedley, Bioconvection in suspensions of oxytactic bacteria: linear theory, *J. Fluid Mech.* 324 (1996) 223–259.
- [18] H. Holden, K.H. Karlsen, K.A. Lie, N.H. Risebro, *Splitting Methods for Partial Differential Equations with Rough Solutions: Analysis and MATLAB Programs*, European Mathematical Society, 2010.
- [19] S. Kalliadasis, J. Yang, A. De Wit, Fingering instabilities of exothermic reaction-diffusion fronts in porous media, *Phys. Fluids* 16 (5) (2004) 1395–1409.
- [20] J. Kim, H.A. Tchelepi, R. Juanes, Stability, accuracy and efficiency of sequential methods for coupled flow and geomechanics, *SPE J.* 16 (02) (2011) 119084.
- [21] A.E. Kolesov, P.N. Vabishchevich, M.V. Vasilyeva, Splitting schemes for poroelasticity and thermoelasticity problems, *Comput. Math. Appl.* 67 (2014) 2185–2198.
- [22] J. Kramer, J. Ravnik, R. Jecl, L. Škerget, Three-dimensional double-diffusive natural convection with opposing buoyancy effects in porous enclosure by boundary element method, *Int. J. Comput. Methods Exp. Meas.* 1 (2) (2013) 103–115.
- [23] H.G. Lee, J. Kim, Numerical investigation of falling bacterial plumes caused by bioconvection in a three-dimensional chamber, *Eur. J. Mech. B, Fluids* 52 (2015) 120–130.
- [24] J. Li, B. Rivière, Numerical solutions of the incompressible miscible displacement equations in heterogeneous media, *Comput. Methods Appl. Mech. Eng.* 292 (2015) 107–121.
- [25] C. López, Z. Neufeld, E. Hernández-García, P.H. Haynes, Chaotic advection of reacting substances: plankton dynamics on a meandering jet, *Phys. Chem. Earth B* 26 (2001) 313.
- [26] M. Marlow, Y. Sasaki, D.A. Vasquez, Spatiotemporal behavior of convective Turing patterns in porous media, *J. Chem. Phys.* 107 (13) (1997) 5205–5211.
- [27] K.W. Morton, *Numerical Solution of Convection-Diffusion Problems*, Applied Mathematics and Mathematical Computation, vol. 12, Chapman & Hall, London, 1996.
- [28] L.E. Payne, J.C. Song, Spatial decay for a model of double-diffusive convection in Darcy and Brinkman flows, *Z. Angew. Math. Phys.* 51 (2000) 867–880.
- [29] L.D. Plante, P.M. Romano, E.J. Fernandez, Viscous fingering in chromatography visualized via magnetic resonance imaging, *Chem. Eng. Sci.* 49 (14) (1994) 2229–2241.
- [30] S. Rothe, P. Erbts, A. Düster, S. Hartmann, Monolithic and partitioned coupling schemes for thermo-viscoplasticity, *Comput. Methods Appl. Mech. Eng.* 293 (2015) 375–410.
- [31] Q. Shao, M. Fahs, A. Younes, A. Makrabi, A high-accurate solution for Darcy-Brinkman double-diffusive convection in saturated porous media, *Numer. Heat Transf. B* 69 (1) (2016) 26–47.
- [32] M. Wakeni, B.D. Reddy, A.T. McBride, An unconditionally stable algorithm for generalized thermoelasticity based on operator-splitting and time-discontinuous Galerkin finite element methods, *Comput. Methods Appl. Mech. Eng.* 306 (2016) 427–451.
- [33] C. Waluga, B. Wohlmuth, U. Rüde, Mass-corrections for the conservative coupling of flow and transport on collocated meshes, *J. Comput. Phys.* 305 (2016) 319–332.
- [34] J.P. Whiteley, A discontinuous Galerkin finite element method for multiphase viscous flow, *SIAM J. Sci. Comput.* 37 (4) (2015) B591–B612.